Hydrogen-Bonded Clusters: A Study of the Elusive Anisole-Ammonia and Anisole-Water 1:1 Complexes

John Lawrence Loman
Marquette University

HYDROGEN-BONDED CLUSTERS: A STUDY OF THE ELUSIVE ANISOLE-AMMONIA AND ANISOLE-WATER 1:1 COMPLEXES

by

John L. Loman, B.S.

A Thesis submitted to the Faculty of the Graduate School,
Marquette University,
in Partial Fulfillment of the Requirements for
the Degree of Master of Science

Milwaukee, Wisconsin

May 2021

ABSTRACT

HYDROGEN-BONDED CLUSTERS: A STUDY OF THE ELUSIVE ANISOLE-AMMONIA AND ANISOLE-WATER 1:1 COMPLEXES

John L. Loman, B.S.

Marquette University, 2021

The hydrogen bond is one of the most important and versatile interactions found in most subsets of chemistry and biology. This interaction is responsible for reactions and characteristic properties of the systems in thereof. This interaction is just one of several available non-covalent interactions that can occur and over the past several decades of molecular spectroscopy studies, the definition of the hydrogen bond has become broader compared to the "classic" definition.

To accurately study the hydrogen-bonding in these systems can be quite challenging due to the size and complexity of the molecules involved, as well as the other interactions that may play a role. In order to study these interactions, model systems containing the isolated conditions for hydrogen bonding similar to their real-world counterparts have been of great use. By studying the strength, geometric orientation, and spectral features of these systems, these types of interactions are better understood.

Of the model systems involved, those containing ammonia and water have been widely studied due to the critical role of the two solvents across all of chemistry, especially biochemistry. In the past few decades, the anisole-ammonia and anisole-water 1:1 complexes, two potential candidates for hydrogen bonding, have been studied. However, these studies have been mostly comprised of initial experimental investigations and low-level theoretical calculations. This leaves some ambiguity as to the exact strength and binding motifs of these complexes.

The focus of this thesis is to identify the shortcomings of the recent literature and answer some of the remaining questions. The ground-state experimental binding energy for the anisole-ammonia complex is reported for the first time via 2-color-resonant 2-photon ionization (2CR2PI) spectroscopy. Through several high-level DFT calculations, the ground-state structure and binding energy are reported and compared to previous literature. Also, the same plethora of theoretical methods were used to explore the complex in the cation-radical state for the first time. Similarly, the same theoretical investigations were employed to study the ground-state and cation radical structure and binding energy were studied for the anisole-water 1:1 complex. The results obtained were then compared to the previous studies.

ACKNOWLEDGMENTS

John L. Loman, B.S.

I would like to begin by thanking God for blessing me with many gifts and opportunities in my life. Through Him, all of this has been possible.

Many people have played a part in this journey and through their guidance and support I have been successful. I would like to begin by thanking my parents, Mary and Larry. Your endless love and support has been (and will always be) at the forefront of everything I do. I thank you both so very much for conversations on the phone and lovely time spent together back home. Whether work had been well or far from it, I was always one call away from two amazing people that would cheer me on no matter what. In that same spirit, I would like to thank my sister and brother-in-law, Kati and Mustafa, along with the rest of my family for always being there to support me. Although we were not able to spend much time together these last couple years, the times we could meet were always extremely special to me. Outside of gatherings, your countless messages of encouragement inspired me to work hard and were greatly appreciated.

Aside from my biological family, I was so very fortunate to make a great family at Marquette as well. Through band, music ministry, the Jesuit community, and the chemistry department, I have made many memories and many life-long friends. All of you have played an important role in my life, whether making me a better student, a better musician, or a better person. Although some of you have been called away from Milwaukee, I love and appreciate every single one of you and will remember these six years spent at Marquette University for the rest of my life.

Last, but certainly not least, I would like to thank my advisor, Dr. Scott Reid, my committee members, Dr. Jier Huang, Dr. Nicholas Reiter, Dr. Qadir Timerghazin, and my lab mates Dr. Damian Kokkin and James Makuvaza. Your guidance, support, and insight have made me a better scientist and have confirmed my love for chemistry.

TABLE OF CONTENTS

LIST OF TABLES

LIST OF FIGURES

CHAPTER 1
INTRODUCTION

The following section gives a brief overview of non-covalent interactions, their role in van der Waals complexes, and some of the common methods used to study these complexes. The nature of van der Waals complexes with ammonia, water as solvent will also be discussed.

1.1 Non-Covalent Interactions and Van Der Waals Complexes

Non-covalent interactions have been extensively examined both by experiment and theory.[1-12] Compared to common intramolecular forces such as ionic, covalent, and metallic bonding, these intermolecular forces are significantly weaker. However, they still are a rather important area of study due to their role in various subfields of chemistry such as biochemistry, crystal-engineering, and protein folding. However, there is still much to learn about the 'real-world' systems where these interactions reside.

Due to the complex nature of these systems (size, photochemical properties, etc), isolating the non-covalent interaction(s) of these systems for study is not feasible. In order to accurately study and understand these interactions, selective isolation of these interactions is necessary. However, by studying model systems that exhibit isolated interactions that are found in these real-world systems, more information can be gained as to how these types of interactions work. These model systems are comprised of two or more molecules in the gas phase held together solely by non-covalent interactions.

One of the strongest non-covalent interactions is the hydrogen bond. Traditionally, the hydrogen bond is thought of as the interaction between the hydrogen on one molecule interacting with the lone pair on either nitrogen, oxygen, or fluorine of another molecule.

However, over time, the idea of a hydrogen bond has been made broader. In this sense, a hydrogen bond can be thought of simply as the interaction between hydrogen and an electron source, such as the π-cloud above an aromatic ring.

1.2 Methods to Study Van Der Waals Complexes

In order to study these systems experimentally, the advent of the supersonic expansion has been incredibly useful.[1, 12-16] A jet expansion into a vacuum allows for the formation of condensed complexes after collisions cease. By seeding the chemicals required into the supersonic expansion, the complexes of interest can be generated and studied. This technique has been a staple of molecular spectroscopy and depending on the conditions and parameters ultimately allows for the generation of any molecular cluster that is bound; these can be homo-molecular or hetero-molecular complexes and be virtually any combination of chromophore, solvent, and carrier gas.

Once the molecular clusters are formed, there needs to be a selective technique to monitor and study only the desired cluster of interest, since there are likely multiple complexes in the free expansion at any moment. By combining time-of-flight mass spectroscopy (TOF-MS) and resonant ionization, this can be achieved. By using this selective technique, the complexes generated can be separated by mass and by spectroscopic profile (if multiple conformers of a specific complex can be formed).

Of the many resonant techniques available, one of the most versatile is resonance-enhanced multiphoton ionization (REMPI). In this method two or more photons are selectively tuned to excite a particular transition of a chromophore and then ionize the excited chromophore. **Figure 1.2-1** shows the schematic for two of the popular REMPI

techniques: 1-color resonant 2-photon ionization (1CR2PI) and 2-color resonant 2-photon ionization (2CR2PI).

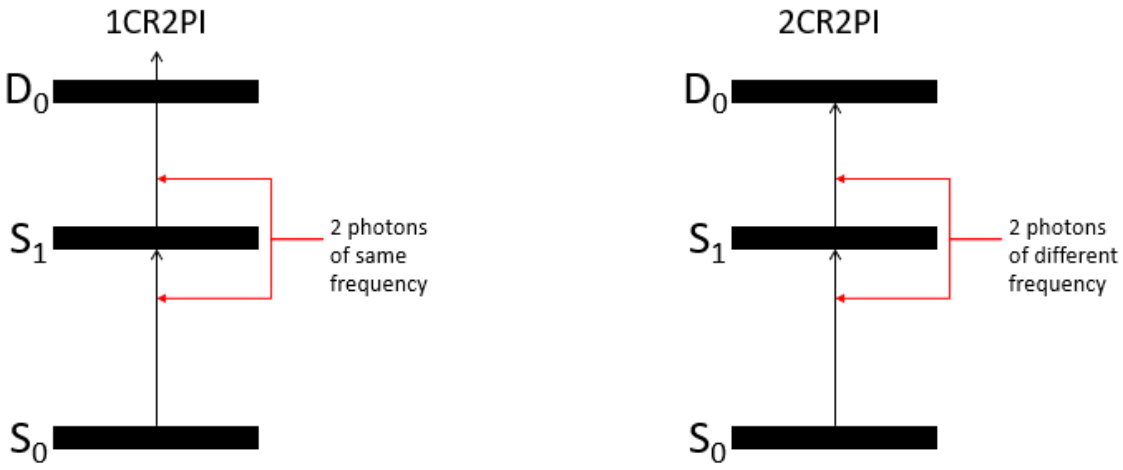

Figure 1.2-1: Schematic of 1-color resonant 2-photon ionization on the left and 2-color resonant 2-photon ionization on the right. In the 1-color schematic, the chemical species absorbs two photons of the same frequency where in the 2-color schematic, the chemical species absorbs one photon of a set frequency and one photon of a different frequency afterwards. This is set with respect to the origin transition, but other transitions may be probed as well.

Both of these techniques allow for selective signal because the first photon is on resonance with a species (and conformer) specific transition frequency. From this, by scanning the first photon frequency and monitoring the ion yield of the chemical species of interest, an excitation spectrum of the chemical species can be achieved. In the case of 1-color method, there is not much additional information that can be gained. However, in the 2-color method due to the tunability of the second photon, additional experiments and spectroscopic information can be gathered.

Some of the major experiments that can be performed using this 2-color method are the determination of the ionization potential (IP), measuring a 2-color appearance potential (2CAP) of the cation fragment of the molecular complex, and velocity mapped imaging (VMI) of the cation fragment of the complex. To measure the IP of the system,

the first photon frequency is set on resonance with the chemical species of interest while the second photon is scanned and the species ion yield is monitored. From here the ionization threshold can be determined by the total energy between the first and second photon. To measure the 2CAP, first photon is set on resonance with the complex species while the second photon is scanned through the ionization threshold while monitoring one of the fragment ion yields. From here the binding energy in the ground state can be determined by taking the total energy of the two photons at the appearance of the cation fragment and subtracting the ionization potential of said fragment. VMI works in a similar way expect instead of creating a spectrum, a camera takes an image of the fragment ions generated as a result of the complex breaking. From taking images at several energy levels above this point, the binding energy of the system can be determined by comparing the size of the integrations relative to the maximum amount of energy from the two photons. These experiments can be used to measure or back-calculate binding energy in respective electronic states for the complex of interest.

To compliment experimental works, many theoretical studies of these systems have been conducted.[9, 12, 17-18] In some cases, when experimental works have been slim or nonexistent, theoretical studies are a great starting point. Of the available tools, theoretical studies often make use of density functional theory (DFT) hybrid methods (such as B3LYP,[19-22] CAM-B3LYP,[23-24] ωB97X-D,[25] M06-2X,[26] PW6B95,[27] PBE0[28-29] etc.) combined with various corrective terms such dispersion energy (Grimme's D3,[30-31] D3BJ[31] are commonly used) if they are not already part of the method. These methods can be used to study many properties including structures and binding interactions, simulate vibrational frequencies, calculate rotational constants, and calculate binding

energies. As a starting point, completing optimization and frequency calculations allows for determination of genuine ground-state minimum structures. From here, various energetic and structural information can be gathered.

1.3 Hydrogen Bonding in Ammonia and Water

Of the many studied molecular complexes, those containing water and ammonia are classic model systems for hydrogen bonding interactions are model systems for the study of hydrogen bonding interactions.[10, 12] These range from small homodimers, trimers etc. to heterodimers with other solvents and chromophores.

Beginning with the simple homodimers, these two complexes exhibit a limited number of possible interactions. For the $(H_2O)_2$ dimer, it has been determined that one water molecule acts a proton donor and one molecule acts as a proton acceptor (at the lone pairs on oxygen) in a quasi-linear orientation.[32] The binding energy of the complex in the ground state has been experimentally determined to be 1105 ± 10 cm^{-1} via velocity mapped imaging (VMI)[33] which is in excellent agreement with high-performance theoretical investigation.[34] As for the $(NH_3)_2$ dimer, there is also a donor/acceptor interaction occurring.[35-39] However, the exact asymmetric structure is not as clear due to complication of a flat PES and large amplitude of motion in available vibrations. Through imaging the ammonia fragments of the dimer, the binding energy was reported to be 660 ± 20 cm^{-1} [40] which was in good agreement with theory.[41-42]

Although these two dimers may seem simple (in terms of being made of two small solvent molecules each), the investigations of these complexes have been anything but simple. This is mostly due to the range of motion and low energy barriers available for said motions. However, one easy deduction to make between these dimers is the

overall strength. The water dimer is bound almost twice as strong compared to the ammonia dimer. This is due to water's ability to better facilitate hydrogen bonding compared to ammonia. Simply put, oxygen is more electronegative than nitrogen.

As we move on from these simple dimers, these solvents can form complexes with aromatic molecules as well. Whether or not classic hydrogen bonding is the dominant interaction involved is a question of experimentation. From previous literature several complexes of aromatic chromophores (such as benzene,[43-48] chlorobenzene,[49] fluorobenzene,[50-51] 1,4 difluorobenzene,[51-52] pyridine,[53-54] phenol,[55-56] napthol,[57-59] aniline,[60-62] etc.) and water or ammonia have been studied. From these systems, a plethora of different types of interactions ranging from in plane, out of plane 'classic' hydrogen bonding, interaction between hydrogen and the aromatic ring were determined. Among these aromatic chromophores, anisole has also been studied with ammonia[63-66] and water.[67-74] Of these studies, it is still ambiguous as to the dominant interaction due to the presence of both the aromatic ring and the electronegative oxygen on the methoxy substitution.

CHAPTER 2
ANISOLE-AMMONIA

This chapter will discuss in detail the previous studies of the anisole-ammonia 1:1 complex, highlighting the major findings and the unanswered or ambiguous questions that remain with respect to binding motif and strength of the complex. In the following sections, the experimental and theoretical studies of the anisole-ammonia complex will be explained in detail.

2.1 Introduction

Table 2.1-1: Summary of the binding energy calculations for the anisole-NH_3 complex from previous literature (All reported binding energies are corrected for ZPE, BSSE unless otherwise mentioned)

Anisole-NH_3 Binding Energy		
Method	**S_0 BE (kJ/mol)**	**S_1 BE (kJ/mol)**
B3LYP / 6-311G++** [63,65]	6.8[a]	-
	2.8	6.2[b]
B3LYP-D / 6-311G++** [65]	13.1	22.8[b]
B3LYP-DM / 6-311G++** [65]	6.6	13.8[b]
M05-2X / 6-311G++** [65]	11.3	17.2[b]
LC-ωPBE / 6-311G++** [65]	7.8	11.6[b]
LC-ωPBE-TPSS / 6-311G++** [65]	7.3	10.7[b]
MP2 / 6-311G++** [65-66]	5.2	-
	9.02	-
MP2CP / 6-311G++** [65]	6.6	-
CCSD / 6-311G++** [65]	3.9	4.7[c]
CCSD(T) / 6-311G++** [65]	5.4	7.1[c]

a. Only corrected for BSSE
b. Calculated from TD-DFT calculation
c. Calculated from EOM calculation

The anisole-NH_3 1:1 complex was first studied by Piani.[63] Using REMPI-TOF spectroscopy, the group found the $S_1 \leftarrow S_0$ origin transition for the complex. Relative to that of bare anisole, the transition was shifted approximately 200 cm^{-1} lower in energy (redshifted). This shift corresponds to a stabilization in the excited state relative to the

ground state. Due to the knowledge of the $\pi \rightarrow \pi^*$ electronic transition of anisole, yielding a shift in electron density from the oxygen of the methoxy substitution into the aromatic ring upon excitation, it was presumed that this complex was bound by non-covalent interactions involving the π-cloud above the ring.

To support their experimental findings, this group carried out molecular dynamics simulations to study the potential energy surface for the system. Starting from the minimum energy structures found in the simulations, subsequent calculations were performed using the B3LYP density functional theory combined with the 6-311G**++ basis set to optimize the structures. From here, 3 candidates were found for the ground-state structure of the complex. From each of the three candidates, a simulation of the excitation spectrum was carried out. The best match to the experimental spectrum was from a conformer where the ammonia molecule sits above plane of anisole and one hydrogen from the solvent interacts with the π-cloud above the ring and one hydrogen from the methoxy substitution interacts with the lone pair on nitrogen. This structure is in agreement with their initial claim that the solvent interacts with the electron density above the ring, but further stabilization from the methoxy substitution was not predicted. The calculated binding energy of this structure was 6.8 kJ/mol, as can be seen in **Table 2.1-1** – it is important to note that this value was only corrected for BSSE.

In a subsequent study,[64] the same group measured high-resolution LIF spectra around the complex origin transition, from which rotational constants, moments of inertia, and structural information about the complex in the ground state and first singlet excited states were derived. The calculated structure in the ground state was in excellent

agreement with their initial assignment and roughly consistent with the predicted structure using dispersion-corrected B3LYP calculations and MP2 calculations.

Barone *et al.* performed further calculations on the complex,[65] using a wider variety of methods to optimize the ground state and first singlet excited state. These include B3LYP (with and without dispersion corrections), M05-2X, PBE with long-range HF exchange (LC-PBE), and MP2 calculations for the ground state and TD-B3LYP (with aforementioned corrections), TD-M05-2X, and TD-LC-PBE calculations for the excited state, as can be seen in **Table 2.1-1**. Upon optimization, further single point calculations were performed using CCSD, CCSD(T) calculations for the ground state and EOM-CCSD, EOM-CCSD(T) calculations for the excited state. These calculations revealed structural and electronic information for the complex as well as sensitivity of the complex binding energy to computational method. For example, in the ground state the calculated binding energy varied from 2.8-13.1 kJ/mol after correcting for ZPE and BSSE. In the excited state, the binding energy varied from 4.7-22.8 kJ/mol after correcting for ZPE and BSSE. Recreating a molecular complex with multiple non-covalent interactions via theoretical study can be quite challenging and binding energies, interaction distances, etc. can change significantly depending on method, basis set, and corrective terms used.

Last, Guiliano *et al.* studied the anisole-NH_3 complex.[66] This group gathered microwave spectra of the complex and then calculated the respective rotational constants. Following this experimental study, the group performed various *ab initio* and DFT calculations on the system. Their MP2 calculation with 6-311++G** basis set yielded rotational constants that were closest to their experimental values. This same calculation yielded a structure that was slightly different than that proposed by Piani.[63] In this

calculated structure, a third non-covalent interaction was evidenced – in addition to the N-H···π and C-H···N interactions, there was a hydrogen of ammonia interacting with the lone pair on the oxygen of the methoxy substitution and increasing the stabilization of the complex in the ground state. This structure, when corrected for ZPE and BSSE, yielded a binding energy of 9.02 kJ/mol, as can be seen in **Table 2.1-1**.

Of the previous studies of the anisole-NH_3 complex, it is agreed upon that the origin transition is approximately 200 cm^{-1} red shifted with respect to bare anisole. It is also agreed upon that there are three non-covalent interactions binding the complex together in the ground state. However, the reported binding energies on this complex are not in unison due to the different theoretical approaches used, as introduced. This exposes the lack of experimentally determined binding energy for the complex in the ground state. Also, there is little information on the complex in the cation radical state. This added information would allow for a benchmark to compare calculated binding energies for the system, as well as better understand the excitation and ionization processes from the ground state of the complex.

2.2 Experimental Procedure

The time-of-flight mass spectrometer used to study the anisole-NH_3 complex has been described previously.[75] Into the source chamber, anisole-NH_3 clusters were formed by passing a 1% sample of ammonia (argon as buffer gas) over a bubbler of anisole, kept at approximately -5 ºC. This mixture flowed through the source chamber of the spectrometer via the 0.8 mm diameter orifice of a General Valve (series 9) pulsed-valve nozzle. This gaseous mixture was then skimnmed by a 1.5 mm Beam Dynamics conical skimmer, effectively making a uniform molecular beam.

This molecular beam was then expanded into the differentially pumped flight tube (via Varian VHS-4 diffusion pump). From here the beam was ionized via a 2CR2PI schematic, which can be seen in the experimental summary in **Figure 2.2-1**. The excitation source (denoted λ_1) came from the frequency-doubled output of a Lambda Physik Scanmate dye laser (pumped by the third harmonic of a Quantel QSmart 850 Nd:YAG laser) and the ionization source (denoted λ_2) came from a Sirah Cobra Stretch dye laser (pumped by a Continuum Indi Nd:YAG laser). λ_1 and λ_2 were aligned counterpropagating to each other and perpendicular to the collimated molecular beam. Using a delay generator (Berkeley Nucleonics), the lasers were temporally overlapped (with λ_1 leading few ns prior to λ_2) and the delay between the nozzle firing and the lasers firing was tuned for optimal signal.

Upon excitation and ionization, the generated ions were extracted and accelerated via a series of three high-voltage electrodes: the extractor electrode held at ~2200 V, the accelerator electrode held at ~1950V, and the third electrode at ground. The accelerated ions then hit a MCP detector and the signal generated was amplified (Stanford Research Systems) and analyzed with a personal computer in a homemade LabView program.

All experimental work was carried out under conditions such that signal found at the anisole-NH_3 ion mass channel was from the generation of the 1:1 complex signal, rather than breakdown product of higher order complexes. First, excitation spectra of anisole-NH_3 complex were measured where λ_2 was kept constant and λ_1 was scanned to the red of the anisole $S_1 \leftarrow S_0$ origin transition while monitoring the ion yield from the complex mass channel. From the excitation spectra, the origin transition of the complex was determined. Last, the two-color appearance potential (2CAP) spectra of the complex

were gathered. Using the method technique explained in **Chapter 1.2**, Anisole cation was generated and monitored from the dissociation of the complex by setting λ_1 on resonance with the complex origin transition while scanning λ_2 above the dissociation threshold of the complex.

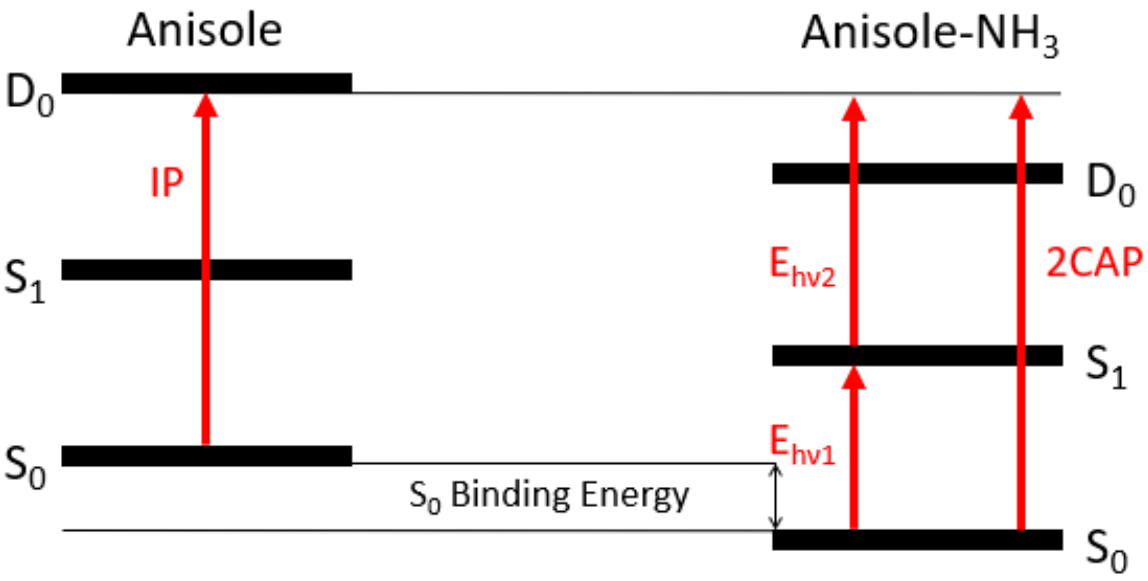

Figure 2.2-1: Summary schematic of experimental parameters studied in relation to anisole and the anisole-NH_3 molecular complex. On the left side are the S_0, S_1, and D_0 electronic energy levels for the chromophore along with the chromophore ionization potential arrow. On the right side similar are the energy levels for the molecular complex along with the 2CAP energy depiction. As shown, two photons, E_{hv1} and E_{hv2}, are used to generate the appearance potential energy. The difference between the chromophore IP and the complex 2CAP yields the labeled S_0 binding energy of the complex.

2.3 Theoretical Procedure

All calculations were performed using the Gaussian 16 (Rev B.01) suite[76] on the XSEDE *Comet* super-computing server.[77]

A variety of DFT single-hybrid methods were used (B3LYP,[19-22] CAM-B3LYP,[23-24] PBE0,[28-29] and M06-2X[26]) in combination with the def2-QZVPPD basis set[78-79] and Grimme's D3 dispersion term,[30-31] due to their success in the past reproducing other hydrogen-bonded van der Waals clusters containing aromatic chromophores.[12] All calculated binding energies were corrected for zero-point energy (ZPE). Due to the size

of the basis set, basis-set superposition error (BSSE) overstabilization was a negligible issue.

Beginning with the neutral ground state fragments, optimization and frequency calculations were performed for anisole and ammonia in order to confirm all structures were minima on the potential energy surface, utilizing the default convergence criteria in Gaussian 16. Afterwards, the same optimization and frequency calculations were performed for the anisole-NH_3 1:1 complex. From here, interaction distances and binding energies were calculated.

For the cation radical state, a similar procedure was used. Unrestricted DFT methods (UB3LYP, UCAM-B3LYP, UPBE0, and UM06-2X) were used in combination with the def2-QZVPPD basis set and Grimme's D3 dispersion term. Optimization and frequency calculations were performed on both the anisole cation and the anisole-NH_3 cation radical. Similar to the analysis of the ground-state structures, binding interaction distances and binding energies were calculated.

2.4 Results and Discussion

The excitation spectrum of the anisole-NH_3 complex is shown in **Figure 2.4-1**.

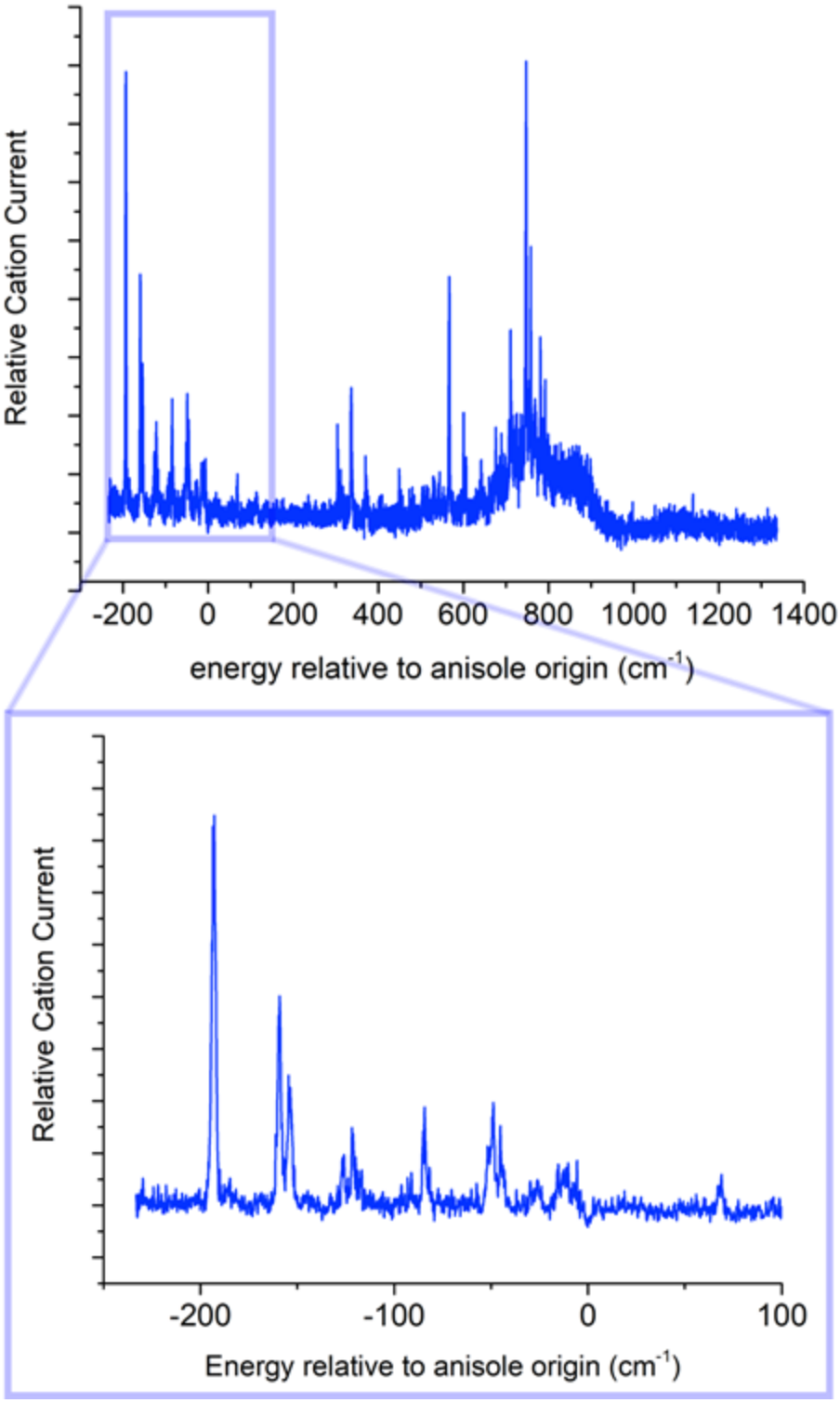

Figure 2.4-1: The excitation spectrum of the anisole-NH_3 complex, relative to the origin transition of anisole. While keeping the ionization laser frequency fixed and scanning the excitation laser frequency, the mass channel of the complex was monitored. The entire spectrum range can be seen in the top figure while the region around the complex origin transition can be seen in the bottom figure.

This spectrum has been made relative by shifting the x-axis with respect to the anisole origin transition, determined by the Reid group previously.[80] Beginning at 193 cm^{-1} to the red of the anisole origin is a large peak, assigned to the origin transition of the complex. This is in agreement with the previous literature.[63] As seen, features continue to appear up to ~1000 cm^{-1} to the blue of the anisole origin transition. These are understood to be anisole modes embedded in the complex excitation spectrum.

After confirming the origin transition of the complex, the 2CAP spectra were taken. As seen in **Figure 2.4-2**, the ion yield of anisole cation is plotted as a function of ground-state binding energy of the complex. From the spectra, two onsets are evident. Using linear extrapolation, the respective intersections of these two onsets yield upper limits to the complex binding energy in the ground state. These intersections correspond to a complex binding energy of approximately 10.2 kJ/mol and to a complex binding energy of approximately 21.6 kJ/mol.

Ammonia has a wagging mode around 950 cm^{-1},[81] which is approximately the difference between the two complex binding energies (11.36 kJ/mol). Therefore, it was determined that the higher energy onset is from anisole cation from dissociation of the complex with ammonia preferentially populating this vibrationally-excited state. Thus, the true upper limit to the complex ground-state binding energy is 10.2 kJ/mol.

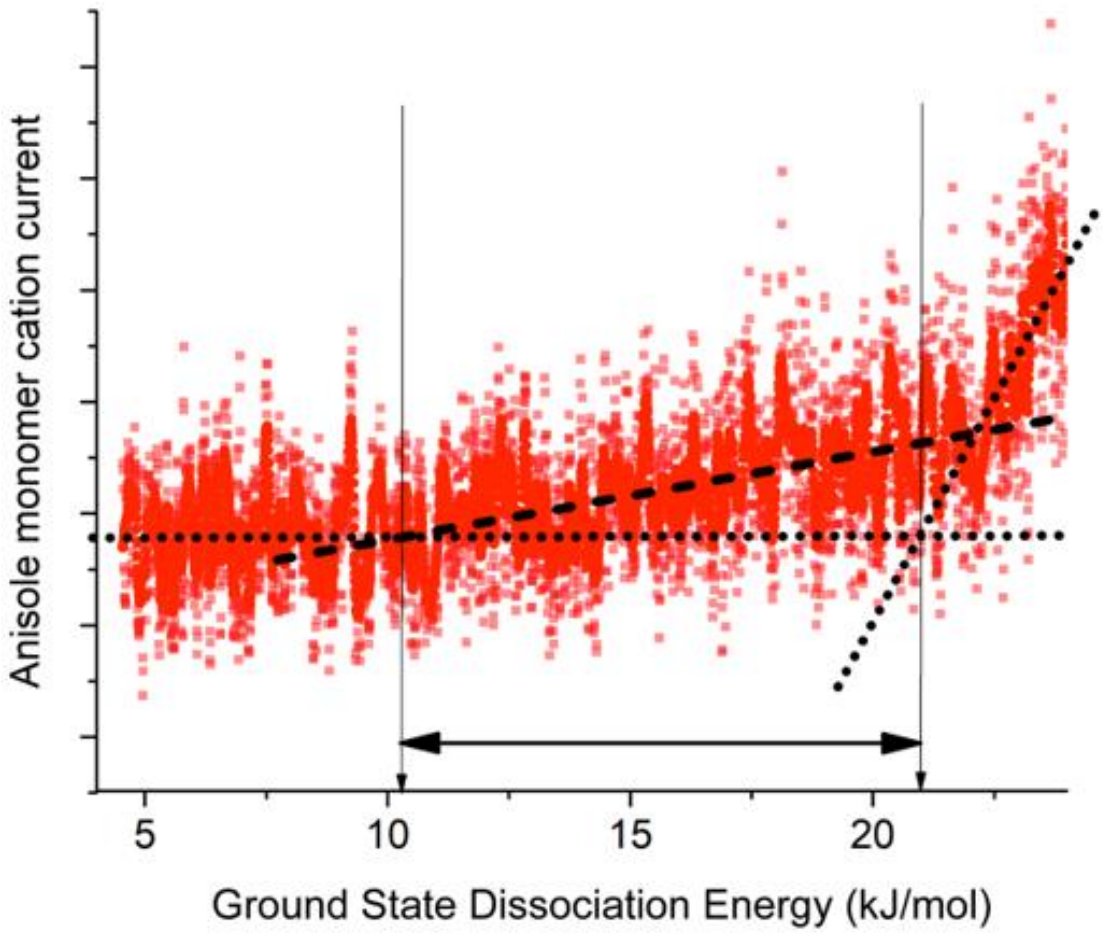

Figure 2.4-2: The 2CAP spectrum of anisole cation yield with respect to anisole-NH_3 ground state binding energy. As featured, there are two linear trendlines, the more gradual one on the left giving the true upper limit of ground-state binding energy and the sharper trendline on the right giving the binding energy of the complex with ammonia populating a vibrationally-excited state.

One caveat with this conclusion is the low signal-to-noise ratio in spectrum which unfortunately adds uncertainty in the reported measurement. However, under the assumption that this is the true ground-state binding energy of the complex, the binding energy in the S_1 state can also be determined by adding the spectral red shift of the complex origin (relative to the origin transition of bare anisole). By adding this additional 193 cm^{-1}, the S_1 binding energy is determined to be 12.6 kJ/mol. This equates to approximately 1050 cm^{-1}.

As stated previously, spectral features cease around 1000 cm^{-1} in the excitation spectrum. This can be understood as the complex dissociating in the S_1 state in this region of the spectrum, thus giving additional support to the previously determined S_0 binding energy derived from the 2CAP spectra. **Figure 2.4-3** shows the expanded region of interest.

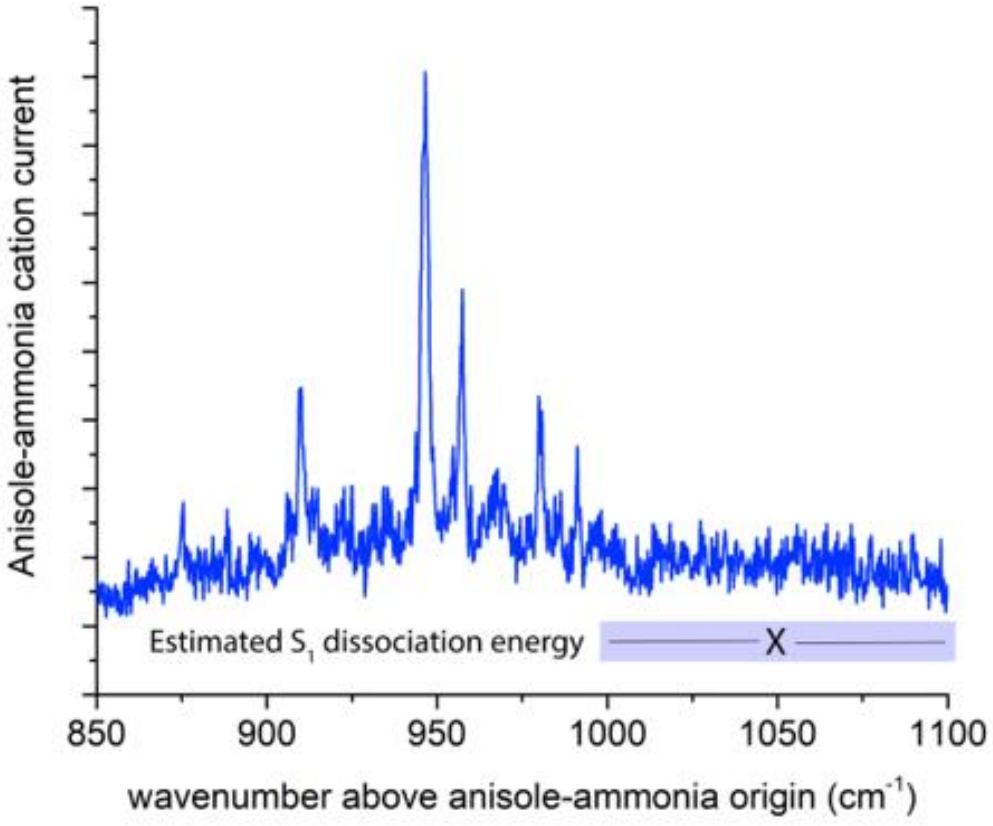

Figure 2.4-3: Expansion of the anisole-NH_3 complex excitation spectrum around 1000 cm^{-1} to the blue of the bare anisole origin transition. The approximated S_1 binding energy of the complex is shown by the X with error bars on either end of the grey region. No obvious modes appear in this area nor past it.

The calculated ground-state structures for the Anisole-NH_3 complex show the presence of 3 non-covalent interactions: N-H···π, N-H···O, and C-H···N. This was consistent among the various methods used to calculate the structure and is good

agreement with the previous work of Guiliano *et al*.[66] This motif can be seen in **Figure 2.4-4**.

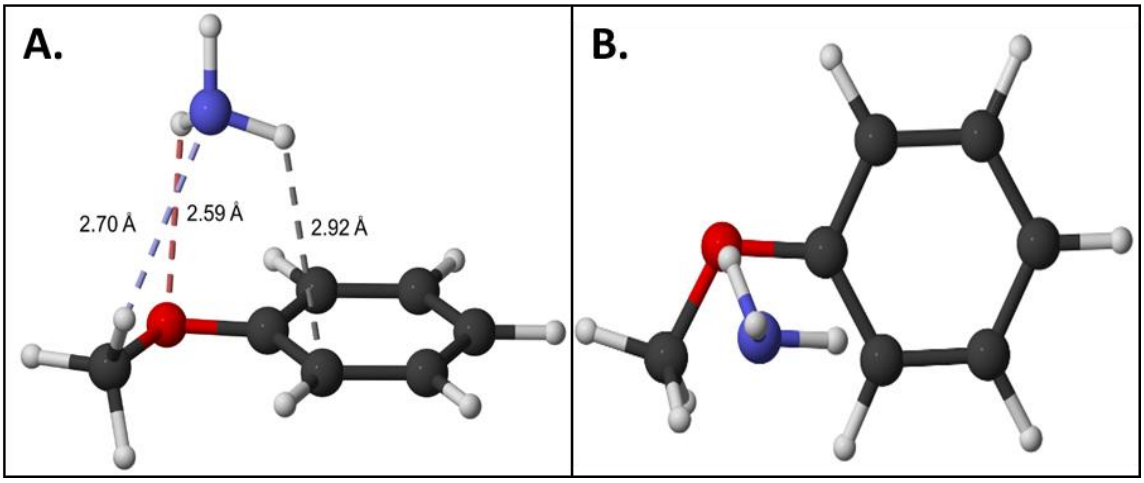

Figure 2.4-4: The calculated ground-state structure for the anisole-NH_3 complex using B3LYP-D3/def2-QZVPPD method. The image on the left gives a side-on view while the image on the right gives a top-down view.

The different methods, while in good agreement with respect to the interaction distances and binding energies, all slightly overestimated the experimental complex binding energy. **Table 2.4-1** shows the summary information from the DFT single-hybrid calculations. As shown, with the exception of the N-H···O interaction in the PBE0 calculation, the interaction distances in increasing order are N-H···O < C-H···N < N-H···π respectively. This would suggest that in this complex, the N-H···O interaction is strongest interaction and the N-H···π is weakest, relatively speaking.

Table 2.4-1: Summary of the ground-state binding energies and interaction distances for the anisole-NH_3 complex between the various calculation methods (All reported binding energies are corrected for ZPE)

Anisole-NH_3 S_0 Binding Energy and Interaction Distances				
Method	**BE (kJ/mol)**	**N-H···π (Å)**	**N-H···O (Å)**	**C-H···N (Å)**
Experimental	10.2	-	-	-
B3LYP-D3 / def2-QZVPPD	11.6	2.92	2.59	2.70
CAM-B3LYP-D3 / def2-QZVPPD	11.8	2.96	2.52	2.68
PBE0-D3 / def2-QZVPPD	12.1	2.87	2.74	2.67
M06-2X-D3 / def2-QZVPPD	12.4	2.86	2.54	2.65

However, for the cation-radical state, there are no previously reported structures nor experimental binding energies in literature for comparison. Here, the cation radical was theoretically analyzed.

When using these same methods, the complex in the D_0 state appears to undergo a significant geometry change into one of two minima. In one conformer (denoted #1), the solvent molecule is centered above the α-carbon of the methoxy substitution where in the other conformer (denoted #2) the solvent molecule is above the para-carbon of the aromatic ring. Also, in both conformers, the solvent is inverted so the nitrogen is now closest to anisole and the three hydrogens are pointed away from anisole. These conformers can be seen in **Figure 2.4-5**.

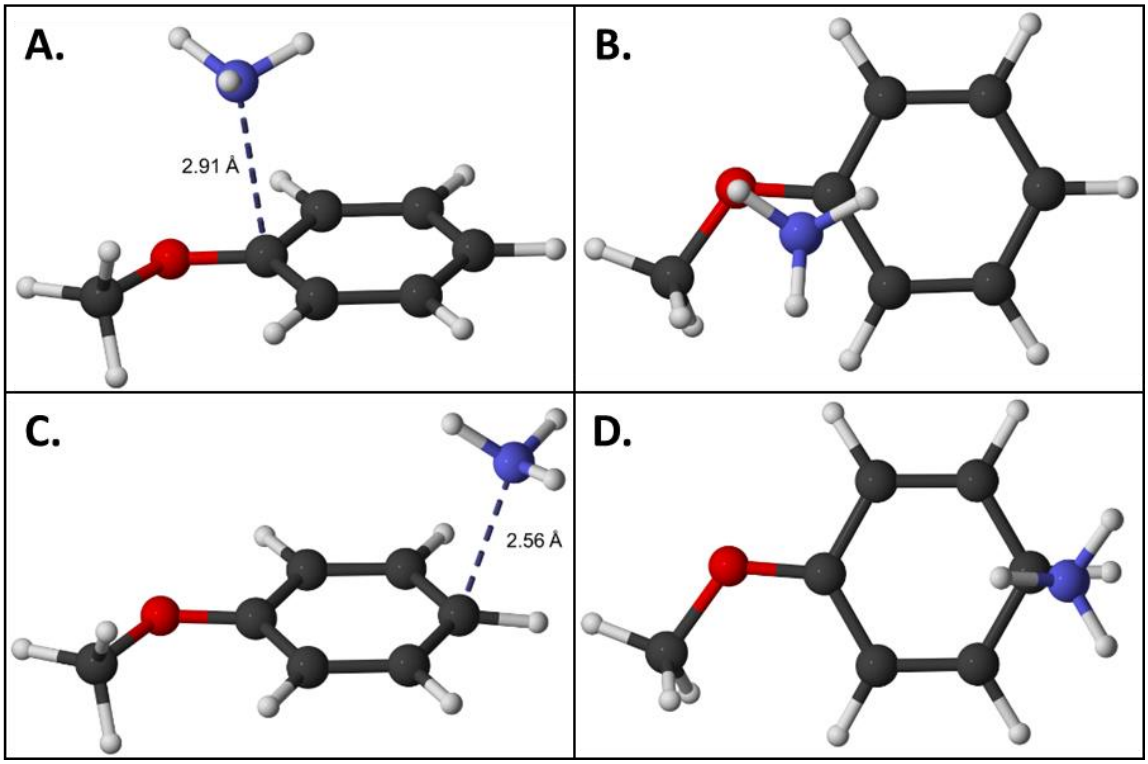

Figure 2.4-5: The calculated cation-radical state conformers for the anisole-NH_3 complex using CAM-B3LYP-D3/def2-QZVPPD method. A gives a side-on view of conformer #1 while B. gives a top-down view of conformer #1. C. gives a side-on view of conformer #2 while D. gives a top-down view of conformer #2.

In these conformers, the main interaction can be thought of as a partial covalent bond forming. In both cases, the increase in binding energy 3-4 times greater compared to the ground state. These calculations suggest that in the cation radical state, the complex is substantially more bound. In the case of conformer #1, the calculated binding energies are in good agreement with each other whereas the binding energies are more spread between calculations for conformer #2. Across both conformers, the interaction distances between nitrogen and the respective carbon are consistent. The calculated binding energies in these two conformers can be seen in **Table 2.4-2.**

Table 2.4-2: Summary of the cation-radical binding energies and interaction distances for the two conformers of the anisole-NH_3 complex between the various calculation methods (All reported binding energies are corrected for ZPE)

Anisole-NH_3 D_0 Binding Energy and Interaction Distances	Conformer #1		Conformer #2	
Method	**Energy (kJ/mol)**	**(α) C···N (Å)**	**Energy (kJ/mol)**	**(p) C···N (Å)**
B3LYP-D3 / def2-QZVPPD	39.3	2.81	39.9	2.58
CAM-B3LYP-D3 / def2-QZVPPD	36.7	2.91	32.5	2.56
PBE0-D3 / def2-QZVPPD	39.8	2.75	40.4	2.46
M06-2X-D3 / def2-QZVPPD	38.0	2.90	33.5	2.63

In order to better understand these structures, Mulliken Charge Maps were produced for the anisole fragment and the complex cation. The fragment cation can be seen in **Figure 2.4-6**. When going from the neutral ground state to the cation radical state, it is apparent that the oxygen loses some of its negative charge while the alpha carbon and the aromatic hydrogens become substantially more electropositive. This is supported by the understanding that from $S_1 \leftarrow S_0$ transition, there is a shift of electron density from the methoxy substitution into the ring. With this understanding in mind, the Mulliken charge map for the complex in the cation state was carried out in **Figure 2.4-7**.

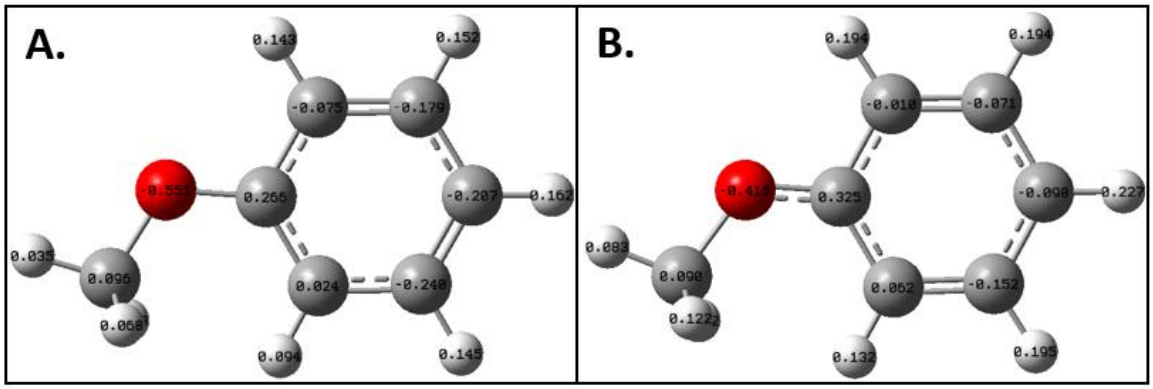

Figure 2.4-6: The calculated Mulliken Charge maps for anisole using CAM-B3LYP-D3/def2-QZVPPD. A. gives the charge map for neutral anisole while B. gives the charge map for anisole in the cation radical state.

For conformer #1, it is clear that the charge density on nitrogen is interacting with the electropositive α-carbon as this aligns with the charge map on the anisole cation fragment. However, for conformer #2, the carbon in the para position becomes more electropositive in this complex in comparison to the anisole cation fragment. Because of this relative increase in positivity, Nitrogen and this aromatic carbon can form an incipient bond.

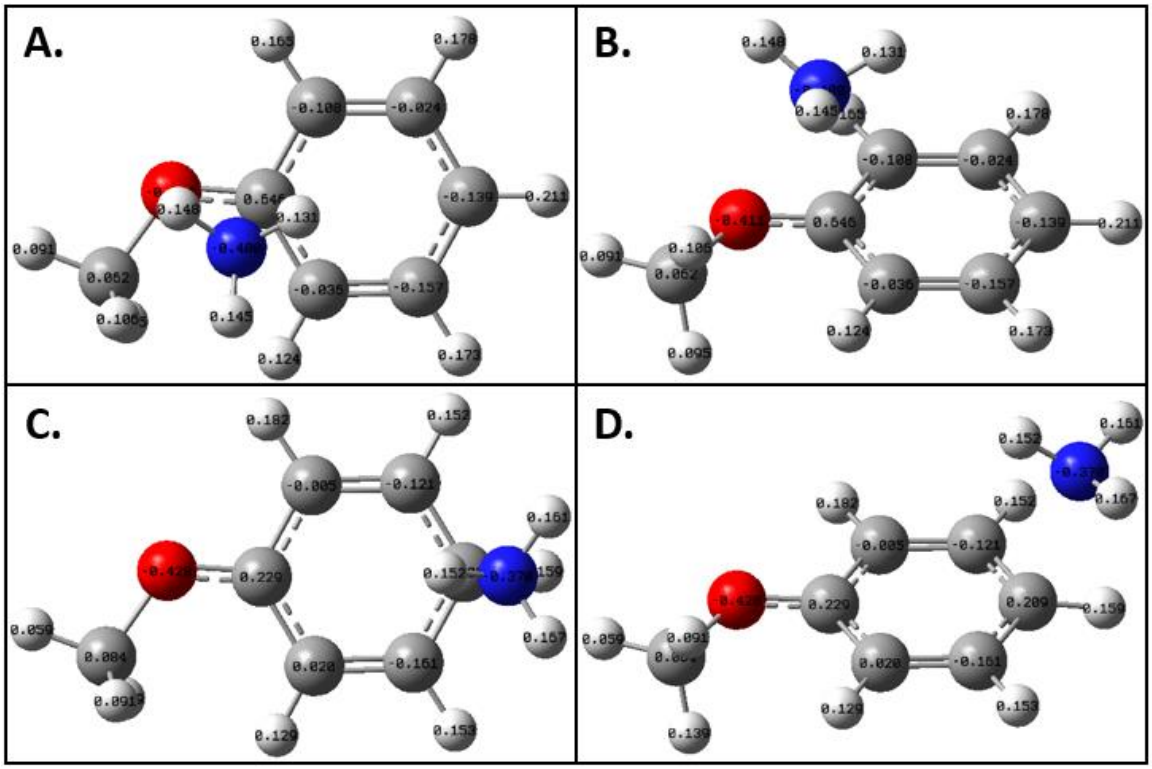

Figure 2.4-7: The calculated Mulliken Charge maps for anisole-NH_3 cation radical conformers using CAM-B3LYP-D3/def2-QZVPPD. A gives a side-on view of conformer #1 while B. gives a top-down view of conformer #1. C. gives a side-on view of conformer #2 while D. gives a top-down view of conformer #2.

While B3LYP and PBE0 DFT calculations give similar charge maps for conformer #1 and #2 (shown in appendix), the M06-2X calculation gave a slightly different contour for conformer #2. As shown in **Figure 2.4-8**, the para-carbon is greatly electronegative in comparison to the respective carbon in the other DFT calculations. With that being said,

the aromatic hydrogen at the para position is extremely electropositive in this calculation. In this scenario, the nitrogen can interact with the greatly electropositive hydrogen. An interesting observation is while the interaction shifts from N··C to N···H between the CAM-B3LYP and M06-2X calculations, the binding energy for the conformer stays roughly the same. Thus, there is some ambiguity between the various DFT calculations for conformer #2.

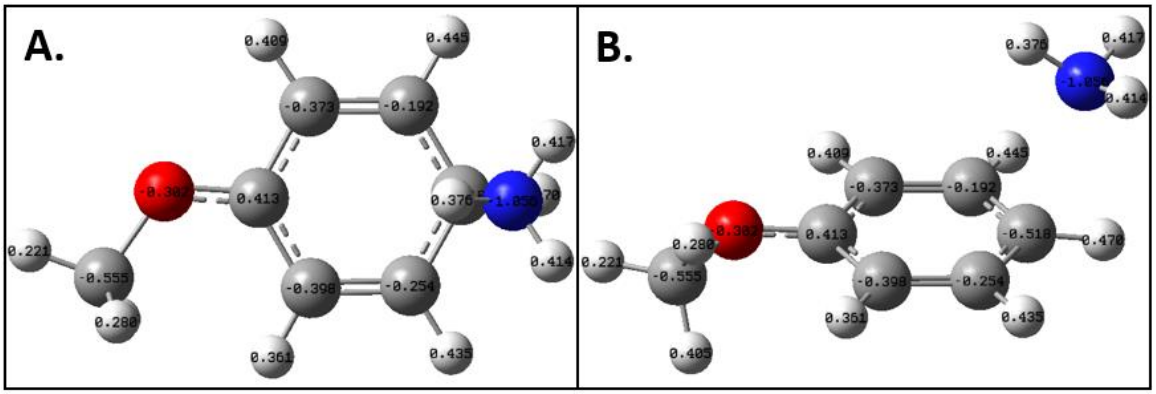

Figure 2.4-8: The calculated Mulliken Charge maps for anisole-NH_3 cation radical conformer #2 using M06-2X-D3/def2-QZVPPD. A gives a side-on view of the conformer while B. gives a top-down view of the conformer.

From charge analysis, both conformers are possible. However, from charge analysis alone, it is not possible to discern which complexes occur in nature. In the previously studied chlorobenzene-NH_3 complex, only one cation radical structure was proposed by the Reid group on the basis of stability post abstraction of hydrogen and HCl.[49] Through calculations, a structure similar to that of conformer #1 supported the experimental findings. However, due to the nature of the studied one-color experiment for this complex, perhaps the extra energy above the ionization threshold preferentially populated the observed reaction pathway as opposed to other structures. In the anisole-NH_3 complex, such thought of a reaction process abstracting methanol or other moieties

was not considered. Perhaps in future studies, a one-color experiment with energy well above the ionization threshold may give additional information to such an occurrence.

2.5 Conclusion

The anisole-NH_3 1:1 complex has been studied. The ground state binding energy has been determined experimentally to be 10.2 kJ/mol via 2CAP spectroscopy which was confirmed by the respective disappearance of vibrational modes in the 2CR2PI spectra for the S_1 excited state. These experimental findings for the ground state were in excellent agreement with DFT calculations; the ground state structure was confirmed to be made of three non-covalent interactions (N-H$\cdots$O, N-H$\cdots\pi$, and C-H$\cdots$N).

The cation radical state of this complex was also theoretically studied using unrestricted DFT calculations for the first time. Two conformers for this electronic state were found: conformer #1 yielded an incipient bond between the nitrogen in ammonia and the α-carbon of anisole where conformer #2 yielded an incipient bond between nitrogen and the para-carbon of anisole. In both cases, ammonia is localized above the plane of anisole and the binding energies increased significantly with respect to the ground state (~30-40 kJ/mol).

This work aimed to advance the understanding of the complex, however, there are still unanswered questions remaining. For example, experimental measurement of the cation radical binding energy should be performed (via imagining or other spectroscopic technique). Also, more information should be gained about the ionization process of the complex, such as determination of the ionization potential.

CHAPTER 3
ANISOLE-WATER

This chapter will discuss in detail the previous studies of the anisole-water 1:1 complex, highlighting the major findings and the unanswered or ambiguous questions that remain with respect to binding motif and strength of the complex. In the following sections, the theoretical studies of the anisole-ammonia complex will be explained in detail. Due to unforeseen circumstances, no experimental studies of the complex were performed.

3.1 Introduction

The anisole-H_2O 1:1 complex was first studied by Barth *et al*.[67] They set out to study the solvation effect of water on benzene and various substituted benzene chromophores. Through IR depletion spectroscopy, spectra around the -OH stretching modes were captured for the complexes and compared to the symmetric and antisymmetric modes of water (which occur at 3657 cm^{-1} and 3756 cm^{-1} respectively). In most cases, the stretching frequencies did not shift much from that of water (most experienced shifts 10-20 cm^{-1}). As justification, Barth *et al.* suggested that the water molecule was not inhibited significantly by the chromophore and therefore was bound in the complex by interaction with the π-cloud.

However, in the case of the anisole-H_2O 1:1 complex, the -OH stretching modes were redshifted significantly from the symmetric and antisymmetric modes of water (66 cm^{-1} and 28 cm^{-1}, respectively). Since the spectrum was drastically different from that of the other water complexes, it was understood that the solvent molecule was being inhibited somehow. Upon further analysis, the -OH frequencies for this complex more

closely resembled the stretching modes of the water dimer where one -OH stretch is participating in hydrogen bonding and the other -OH stretch is 'free' (3601 cm^{-1} and 3735 cm^{-1}, respectively). Therefore, the group proposed that the solvent molecule was interacting with the oxygen on the methoxy substitution of anisole where one -OH is hydrogen bonding to the lone pair and the other -OH is not participating in bonding.

The group went on to further study the anisole-H_2O complex to better understand this phenomenon.[68] In this study, they began by reporting the excitation spectrum for the complex. From this, they determined the origin to be approximately 118 cm^{-1} blue-shifted compared to anisole. Also, the group went on to perform calculations to try and reproduce the observed -OH stretching modes of the complex and gain additional structural insight. The modes were best reproduced with MP2 calculations combined with 6-31+G* basis set, and the optimized structure was carried out using MP2 calculations with aug-cc-pVDZ basis set. These calculations show the water molecule above the plane of anisole with one hydrogen from water bonding with the lone pair on oxygen of anisole and the other hydrogen out of the plane of interaction, as predicted. The group also calculated the ground-state binding energy of this structure to be 3.58 kcal/mol. They commented on how close this was in strength to the reported binding energy of the water dimer at the time. Altogether, they used this information to strengthen their initial claim that the water molecule binds to the oxygen of anisole and overall behaves similarly to the water dimer.

Unfortunately, this theoretical study was found to be flawed. While reproducing IR frequencies via calculation can be achieved quite easily, even using poor levels of theory and extremely small basis sets, the reported structure needs additional support.

Also, the reported binding energy was not corrected for BSSE; it was only corrected for half of the overstabilization due to BSSE. When using very small basis sets, this term is normally quite large. When the entire BSSE correction is made, the binding energy of the complex is 2.15 kcal/mol which is significantly smaller than reported.

Despite the issues with this entrant, other groups would go on to study the complex as well. Becucci *et al.* made use of high-resolution spectroscopy to gain more experimental insight into the complex.[69] The group first used REMPI to confirm the origin transition of the complex. Once done, they collected rotationally resolved spectra around the origin. From this, rotational constants were calculated, and a structure was established. This one, similarly to the previously reported structure, involved one hydrogen of water hydrogen bonding to the lone pair on the methoxy substitution with the other hydrogen from water 'free'. However, the hydrogen bond in this structure was in the plane of anisole, as opposed to the previously reported out-of-plane structure.

After this finding, the group carried out a theoretical study.[70] Using a standard Molecular Mechanics software, the group simulated the potential energy surface of the complex; all minima were identified. From these minima, optimization calculations were carried out using the B3LYP Density Functional Theory combined with the 6-311++G(d,p) basis set. As a result, 7 potential conformers were found for the ground state, which fell into one of three binding motifs: 1. Hydrogen from water interacting with the π-cloud above the ring, 2. Hydrogen from water interacting with the lone pair of oxygen from the methoxy substitution, or 3. Hydrogen from the methoxy substitution interacting with a lone pair of oxygen in water. The conformers from the first group yielded the strongest calculated binding energy, while conformers from the third group

yielded the weakest calculated binding energy. Within each group, the conformers yielded extremely similar binding energies. Before deductions were made, the group simulated the rotational contour around the origin transition for each type of conformer. The only simulation that resembled the experimental spectrum was that of the second conformer type.

The group then suggested that the water molecule does in fact undergo a linear hydrogen bond to the lone pair of the oxygen of the methoxy substitution. They also suggested that the hydrogen bond is at least quasi planar with respect to anisole. However, exact placement of the water molecule was not possible by this method. On top of this ambiguity, the group found two clusters of peaks at the origin transition separated by ~0.2 cm^{-1}. The group ascribed these two sets of peaks as to some sort of internal motion but did not comment further.

To clear some of this confusion of the structure and claimed internal motion, Giuliano *et al.* used microwave spectroscopy to study various deuterated conformations of the anisole-H_2O complex.[71-72] Under the null assumption that the molecular structure of the complex would not change upon deuteration, the microwave spectra of anisole-H_2O, anisole(d3)-H_2O, anisole(d5)-H_2O, anisole-DHO, and anisole-D_2O were gathered. This assumption was found to be true when deuterating the methyl and aromatic hydrogens on anisole.

However, when deuterating the hydrogens on water, it was clear that there were non-negligible geometry changes for the complex. When studying the microwave spectra of anisole-H_2O, anisole-DHO, and anisole-D_2O, it appeared that there was an additive change on the geometry of the complex: specifically when looking at the angle between

the α-carbon, the oxygen of the methoxy substitution and the oxygen of water. When going from anisole-H_2O to anisole-DHO to anisole-D_2O, the angle decreased while maintaining approximately the same distance between the oxygen from the methoxy group and the oxygen of water. This caused the distance between the oxygen of water and the closest methoxy hydrogen to increase upon deuteration and the distance between oxygen of water and the closest aromatic hydrogen to decrease upon deuteration.

Due to this additive change in angle and the observed splitting around the origin, it was assumed that the hydrogens on water had equal impact on the structure and spectral information of the complex. Therefore, this group proposed that the splitting was due to a rocking motion of the water molecule around a bifurcated transition-state where each hydrogen of water was equally interacting with the lone pair of oxygen on anisole. On either side of this transition state would be local minima where one hydrogen from water hydrogen-bonds to the lone pair on oxygen in plane

This would serve to be sensible explanation. However, Ribblett *et al.* would go on to challenge this claim.[73] They also studied these two sets of peaks. From the relative intensities (~3:1), they suggested that this is due to the solvent undergoing a hindered motion that results in an exchange of the two hydrogens. They support this claim by discussing similar occurrences of a 2-step motion observed in the benzonitrile-H_2O, p-difluorobenzene-H_2O, and indole-H_2O complexes.[82-84]

This two-step motion begins with a slightly different orientation of the solvent molecule. While there is still a hydrogen bond between a hydrogen of water and the lone pair from the oxygen of the methoxy substitution occurring in plane, a lone pair from oxygen in the solvent interacts with the closest neighboring C-H bond from the aromatic

ring. This creates a sense of two hydrogen bonds occurring at the same time. From this starting geometry, the hydrogen from the solvent not participating in bonding begins orientated on one side of the plane of anisole and then inverts to the opposite side. From here, the solvent rotates about the oxygen, thus switching the placement of the two hydrogens. This process would occur back and forth allowing for the two hydrogens from water to be equivalent, as was discussed by Giuliano.

With conflicting ideas, Pasquini *et al.* performed calculations on the ground-state and first excited state for the complex.[74] From here they also carried out calculations to determine the energy required for the proposed mechanism of Giuliano and Ribblett. F. For Giuliano, the bifurcated structure was confirmed as a genuine transition state (through use of IRC calculations) with a linear hydrogen-bond in plane as local minima on either side. The activation energy to achieve this transition state was determined to be ~6 kJ/mol. In comparison, the energy of Ribblett's two-step internal conversion was calculated to be ~23 kJ/mol. While this is not confirmatory, this gave more support for the previously proposed mechanism causing the emergence of the two sets of peaks.

In the anisole-H_2O complex, it is agreed upon that the origin transition is approximately 118 cm^{-1} blue shifted with respect to bare anisole. Also, the structure of the complex in the ground state is somewhat agreed upon. The ambiguity in structure arises from the lack of sensitivity in rotational studies. The rotational constants vary with respect to moment of inertia and since the center of mass on water is placed on the oxygen, the exact placement of the hydrogens have minimal effect on rotational constants.

Also, similarly to the anisole-NH_3 1:1 complex, the reported binding energies are significantly different from one another. Theoretically, the calculations that have been performed are not suitable for large conclusions due to the use of small basis sets and lack of dispersion, primarily. Variations in binding motif could yield changes in binding energy that could be monitored experimentally and theoretically. From an experimental determination of the binding energy in the ground state, a benchmark could be set for future calculations of higher computational quality as well as added evidence for an unambiguous structural assignment of the complex. Last, there has been no studies of the cation radical for this complex which would yield insight into the ionization process of the complex.

3.2 Theoretical Procedure

All calculations were performed using the Gaussian 16 (Rev B.01) suite[76] on the XSEDE *Comet* super-computing server.[77]

Similarly to the anisole-NH_3 work, DFT single-hybrid methods were used (B3LYP,[19-22] CAM-B3LYP,[23-24] PBE0,[28-29] and M06-2X[26]) in combination with the def2-QZVPPD basis set[78-79] and Grimme's D3 dispersion term,[30-31] due to their success in the past reproducing other hydrogen-bonded van der Waals clusters containing aromatic chromophores.[12] All calculated binding energies were corrected for zero-point energy (ZPE). Due to the size of the basis set, basis-set superposition error (BSSE) overstabilization was a negligible issue.

Beginning with the neutral ground state fragments, optimization and frequency calculations were performed for anisole and water in order to confirm all structures were minima on the potential energy surface, utilizing the default convergence criteria in

Gaussian 16. Afterwards, the same optimization and frequency calculations were performed for the aniolse-H_2O 1:1 complex. From here, binding interaction distances and binding energies were calculated.

For the cation radical state, a similar procedure was used. Unrestricted DFT methods (UB3LYP, UCAM-B3LYP, UPBE0, and UM06-2X) were used in combination with the def2-QZVPPD basis set and Grimme's D3 dispersion term. Optimization and frequency calculations were performed on both the anisole cation and the anisole-H_2O cation radical. Similar to the analysis of the ground-state structures, binding interaction distances and binding energies were calculated.

3.3 Results and Discussion

The calculated ground-state structures for the anisole-H_2O complex are comprised of a linear hydrogen bond between one hydrogen of the solvent and the lone-pair on oxygen of the methoxy substitution, which is in agreement with Beccuci *et al.*[69] This can be seen in **Figure 3.3-1**.

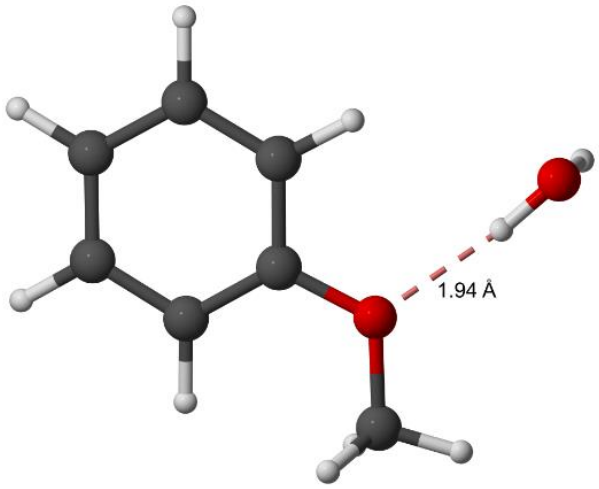

Figure 3.3-1: The calculated ground-state structure for the anisole-H_2O complex using M06-2X-D3/def2-QZVPPD method.

Summarized in **Table 3.3-1** are the DFT calculated ground state binding energies and interaction distances for the anisole-H_2O complex. The binding energy values vary slightly between methods but similar to the structure, are in good agreement with the calculated values of Becucci *et al*. However, in comparison to the ground state anisole-NH_3 binding energy, there are no reported experimental binding energies for anisole-H_2O in the ground state to use as a benchmark. With that being said, under the assumption that DFT hybrid methods reproduce the complex well and accurately, these calculated values should give a good approximation for the true ground-state binding energy.

Table 3.3-1: Summary of binding energies and interaction distances for the anisole-H_2O complex between the various calculation methods (All reported binding energies are corrected for ZPE)

Anisole-H_2O S_0 Binding Energy and Interaction Distance		
Method	**BE (kJ/mol)**	**O-H···O (Å)**
B3LYP-D3 / def2-QZVPPD	15.3	1.92
CAM-B3LYP-D3 / def2-QZVPPD	16.7	1.89
PBE0-D3 / def2-QZVPPD	14.5	1.92
M06-2X-D3 / def2-QZVPPD	13.1	1.94

Similar to the cation radical state of the anisole-NH_3 complex, the geometry of the anisole-H_2O complex drastically changes in the cation radical state compared to the ground state. In one conformer (denoted #1), the solvent molecule shifts from in plane, to above the α-carbon of the methoxy substitution where in the other conformer (denoted #2), the oxygen of the solvent molecule stays in plane with anisole but shifts in between neighboring ortho and meta carbons on the aromatic ring. In both cases, similar to ammonia, water is inverted so that the oxygen of water is interacting with anisole and the hydrogens are pointed away. These conformers can be seen in **Figure 3.3-2**.

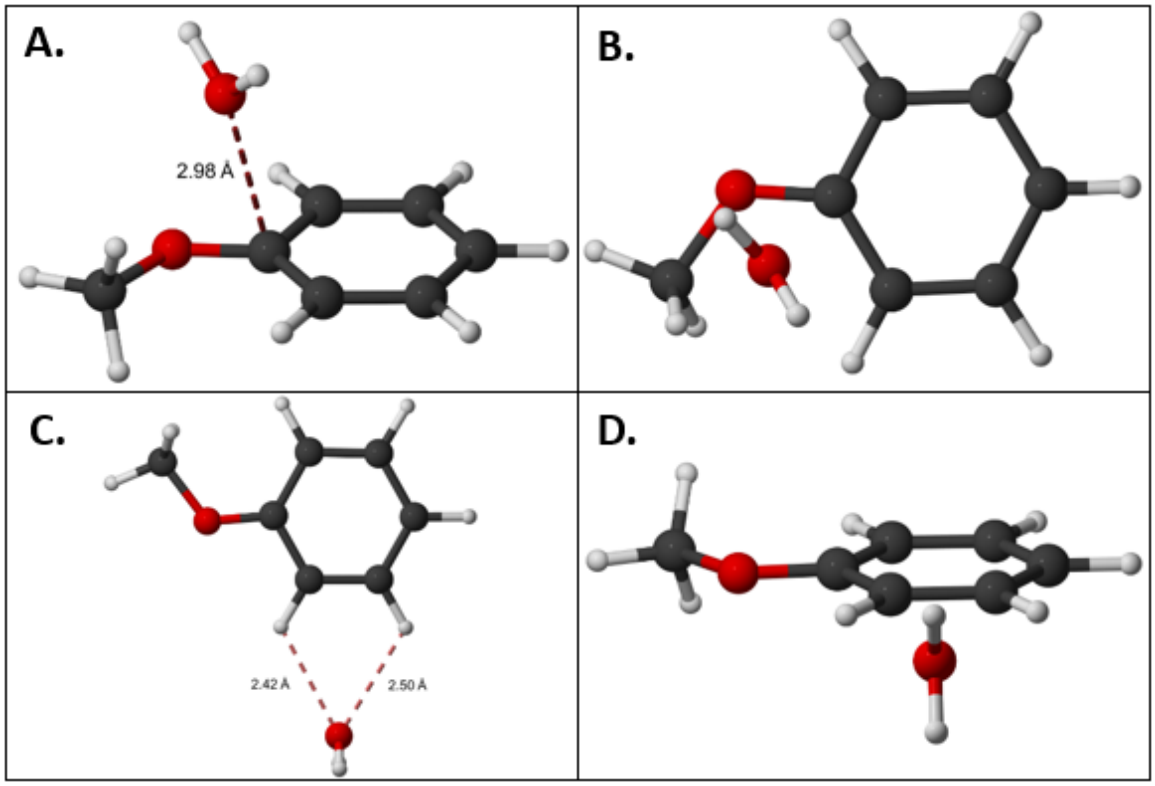

Figure 3.3-2: The calculated cation-radical state conformers for the anisole-H_2O complex using B3LYP-D3/def2-QZVPPD method. A gives a side-on view of conformer #1 while B. gives a top-down view of conformer #1. C. gives a side-on view of conformer #2 while D. gives a top-down view of conformer #2.

Similar to the anisole-NH3 cation radical conformers, the main interaction in conformer #1 and #2 can be thought of as an incipient bond forming between the lone pair of oxygen and a region of electropositivity. In both conformers, the same increase in binding energy is found as is the case for the calculated binding energies for anisole-NH_3 in the cation radical state. However, for the anisole-H_2O complex, the calculated binding energies are in good agreement within each conformer. Both yield similar strengths with conformer #1 having a slightly larger binding energy compared to conformer #2. These binding energies can be seen in **Table 3.3-2**.

Table 3.3-2: Summary of the cation radical binding energies and interaction distances for the two conformers of the anisole-H_2O complex between the various calculation methods (All reported binding energies are corrected for ZPE)

Anisole-H_2O D_0 Binding Energy and Interaction Distances	**Conformer #1**		**Conformer #2**	
Method	**Energy (kJ/mol)**	**(α) C···O (Å)**	**Energy (kJ/mol)**	**C-H···O (Å)[a]**
B3LYP-D3 / def2-QZVPPD	33.3	2.98	29.9	2.42, 2.50
CAM-B3LYP-D3 / def2-QZVPPD	35.0	2.93	31.3	2.39, 2.48
PBE0-D3 / def2-QZVPPD	33.5	2.98	30.2	2.40, 2.51
M06-2X-D3 / def2-QZVPPD	35.2	2.84	29.8	2.38, 2.45

a. Distances listed are between oxygen and hydrogen at the ortho position and at the meta position, respectively.

In similar light to the anisole-NH_3 complex in the cation radical state, Mulliken Charge maps were calculated for the anisole-H_2O complex. As shown in **Figure 3.3-3** both conformers were studied. For conformer #1, we see a similar trend to conformer #1 for the anisole-NH_3 cation radical where the electronegative region of the solvent (in this case the lone pair from the oxygen) interacts with the electropositive α-carbon in the anisole cation fragment discussed in the previous chapter. However, for conformer #2, the oxygen interacts which the electropositive hydrogens on the ortho and meta positions of the aromatic ring. One observation that is surprising is that this localized electropositivity is not as strong as the para position hydrogen, yet the structure optimized at the location it did. This leads to ambiguity and need for further experimental study to understand the possible motifs for the cation radical state.

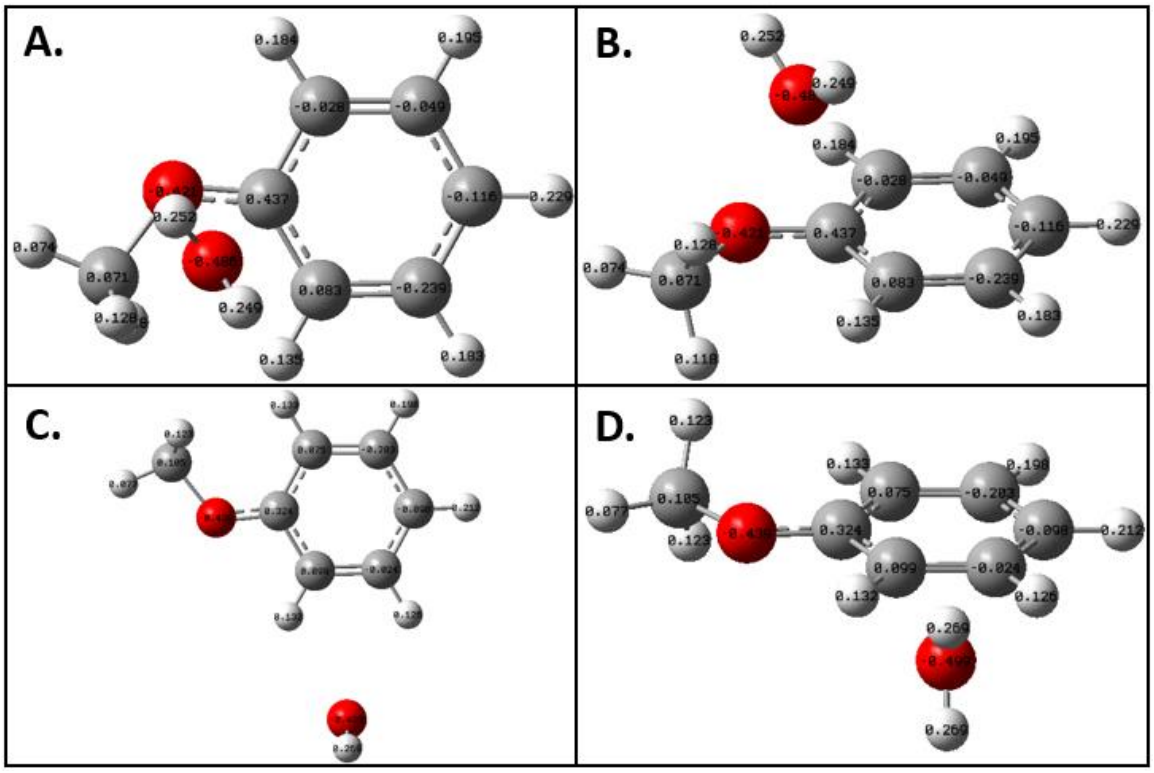

Figure 3.3-3: The calculated Mulliken Charge maps for anisole-H_2O cation radical conformers using B3LYP-D3/def2-QZVPPD. A gives a side-on view of conformer #1 while B. gives a top-down view of conformer #1. C. gives a side-on view of conformer #2 while D. gives a top-down view of conformer #2.

3.4 Conclusion

Theoretically, the ground state structure for the anisole-H_2O complex was studied. The DFT calculations agree with the previously determined structure where there is a linear hydrogen bond between one hydrogen from water and the lone pair of oxygen in anisole, with the solvent molecule in plane. The ground state binding energy calculations were in decent agreement between methods and yielded a value around 13-16 kJ/mol. The cation radical state calculations of this complex, much like that of the anisole-NH_3 complex, yielded a large change in geometry. Again, two conformers were found: conformer #1 suggested an incipient bond between the oxygen of water and the α-carbon above the plane of anisole where conformer #2 suggested an incipient bond between the oxygen of water and the ortho and meta carbons of anisole with the solvent in plane.

Similarly, the binding energies drastically increased compared to that of the ground state. (~30-35 kJ/mol).

This work aimed to advance the understanding of the complex, however, more experiments should be carried out. For example, the ground state binding energy should be measured experimentally, along with the cation radical binding energy (via 2CAP, imaging experiments). Also, more information about the ionization process should be gathered.

CHAPTER 4
COMPARISON & CONCLUSION

This chapter will discuss the results of chapter 2 and chapter 3 in terms of a direct comparison, as well as how they pertain to future research of micro-solvated aromatic complexes.

4.1 Comparison of Results

The studies of the anisole-NH_3 complex and anisole-H_2O 1:1 complexes have yielded very interesting results. Both complexes possess rather different types of hydrogen bonding in the ground state. As determined, ammonia binds with anisole by three ‘unusual’ hydrogen bonds where water binds with anisole via a traditional, linear hydrogen bond. Despite having different binding motifs, the strengths of the two complexes are similar (comparing theoretical calculations), showcasing the strength of a traditional hydrogen bond compared to the ‘unusual’ hydrogen bond.

In the D_0 state, theory predicts that both complexes undergo large changes in geometry. In the calculated structures for both complexes, the solvent molecules invert such that the heteroatom is interacting with anisole and the hydrogens are pointed away. In the case of the anisole-NH_3 complex, this agrees with the analysis of **Figure 2.4-2.** If the intersection at higher complex ground state energy is due to the population of the ammonia wagging mode, then the solvent would tend to orient itself in this manner. However, there is no such evidence to support conformer #1 for anisole-H_2O.

Also in the D_0 state, both complexes undergo a large increase in binding energy. While not as large of increase in the case of anisole-H_2O, both complexes yield

substantial stabilization in the cation-radical state, such that the formation of an incipient bond is suggested, rather than stabilization by weak intermolecular interaction.

4.2 Future Experiments

These experimental and theoretical findings for the anisole-NH_3 and anisole-H_2O complexes support and enhance the previous literature.[63-66, 67-74] However, to better understand these complexes, further investigation is necessary.

For the anisole-NH_3 complex, the experimentally determined ground-state binding energy served as an excellent benchmark to compare theory. A similar approach should be used for the cation-radical state. This can be achieved easily by one of two methods.

By experimentally determining the ionization potential of the complex, the binding energy in the D_0 state can be returned from use of a thermochemical cycle, like **Figure-2.2-1**. The IP can be determined via the same experimental setup used here: TOF-MS combined with 2-color resonant ionization. By probing the complex with the first photon set on resonance with the $S_1 \leftarrow S_0$ transition and monitoring the complex ion yield with the second photon scanned through the ionization threshold, an upper limit to the IP can be determined. From here, the cation radical can be determined by subtracting the complex IP from the combined total energy of the anisole IP and complex S_0 binding energy.

Also, the cation radical can be determined via imaging the anisole fragment of the complex, as previously used in the study of the anisole-CH_4 and aniline-CH_4 systems.[80,85] In a similar manner to determining the 2CAP spectra of the complex, anisole fragments can be generated by probing the complex on resonance with the $S_1 \leftarrow S_0$ transition while setting the ionization photon at high enough energy above the ionization threshold. From here, an integration of the fragment can be gathered using a camera as a detector. The

image of the fragment ion can then be transformed mathematically into velocity domain from its pixel domain. This can be converted to a kinetic energy distribution and image size analyzed as a function of total energy. From here, the binding energy in the cation radical state can be calculated by subtracting the combined energy of the two photons from the total kinetic energy of the image.

The results from these two techniques can be compared and then used as a benchmark to compare to theory. With that said, additional calculations for the cation radical can be carried out, such as calculations using DFT double-hybrid methods or calculations using different dispersion terms.

As for the anisole-H_2O complex, the reported experimental technique of **Chapter 2.2** should be carried out. First, the $S_1 \leftarrow S_0$ transition of the complex should be combined by setting the second photon constant while scanning the first photon through the region from the previous literature.[67-69] From here, the ground state binding energy should be determined via gathering a 2CAP spectra. By setting the excitation laser on resonance with the determined $S_1 \leftarrow S_0$ transition, the second photon can be scanned above the ionization threshold while monitoring the anisole cation yield. From the spectra, the binding energy of the complex can be calculated and compared to the theoretically determined binding energies. Also, the cation radical can be studied via the same IP and VMI experiments outlined in this section for the anisole-NH_3 complex.

4.3 Outlook

The scope of this work was to enhance the previous investigations of the anisole-NH_3 and anisole-H_2O complexes. However, these are just two complexes of the possible model systems to study. These complexes give insight into -OH and -NH interactions that

exist in nature. However, there are many other types of interactions that ammonia and water can model. Studying how the water, ammonia dimers interact with anisole could be of great use as to understand competing interactions between the various potential hydrogen bonds.

These same types of interactions could be also studied with other aromatic chromophores. As previously stated, many other micro-solvated chromophores have been studied.[43-62] Looking at higher order complexes could be of interesting study to learn how the substitution(s) on the chromophore play a role in the formation of said complexes. Also, looking at aromatic dimers that undergo π-stacking and their solvation with ammonia and water would be of interesting study to look at the competition between π-staking and hydrogen bonding.

These suggestions are just a few related studies to the previous project and highlight the plethora of experimental and theoretical investigations that are possible. Through these projects, the real-world interactions that are modeled can be better understood.

APPENDIX: ADDITIONAL FIGURES

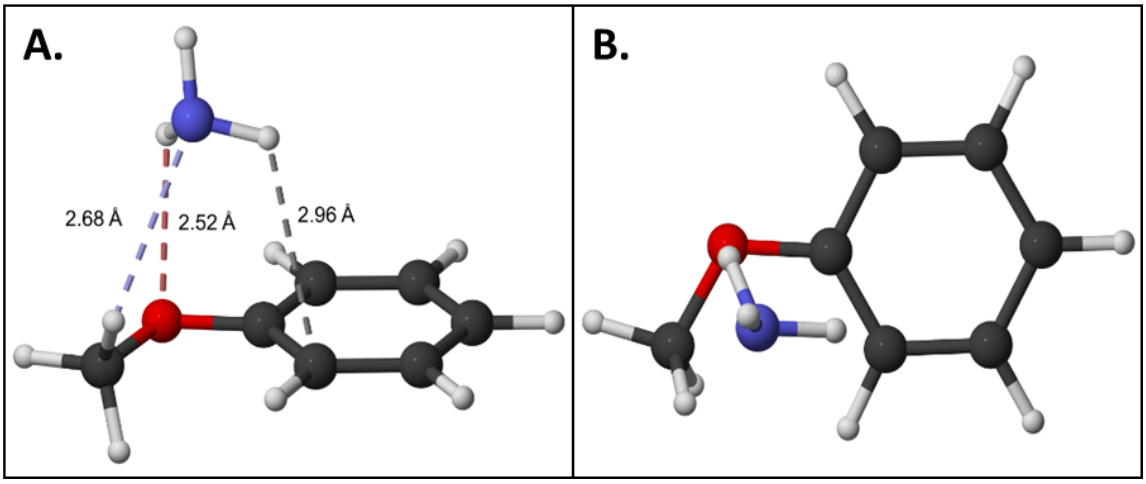

Figure A-1: The calculated ground-state structure for the anisole-NH_3 complex using B3LYP-D3/def2-QZVPPD method. The image on the left gives a side-on view while the image on the right gives a top-down view.

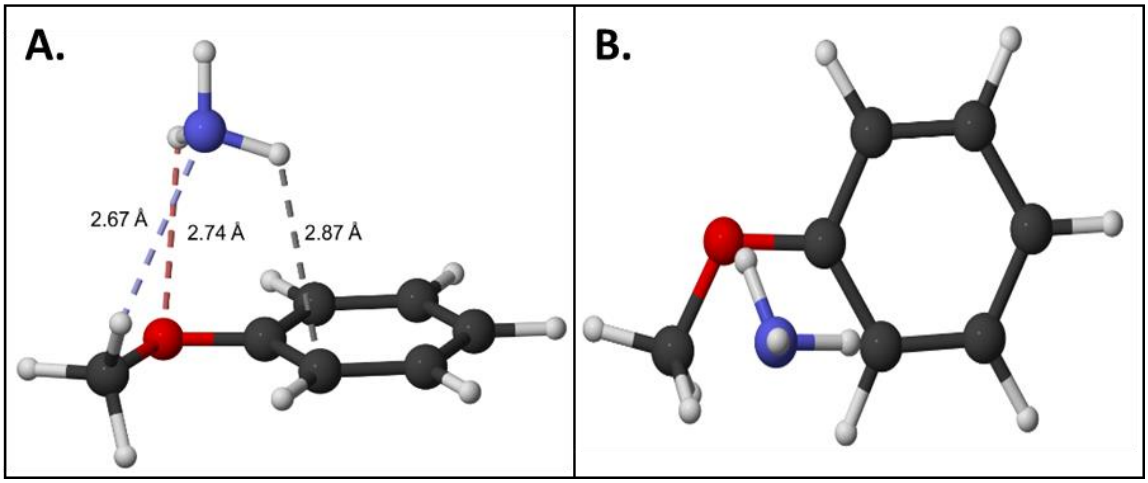

Figure A-2: The calculated ground-state structure for the anisole-NH_3 complex using PBE0-D3/def2-QZVPPD method. The image on the left gives a side-on view while the image on the right gives a top-down view.

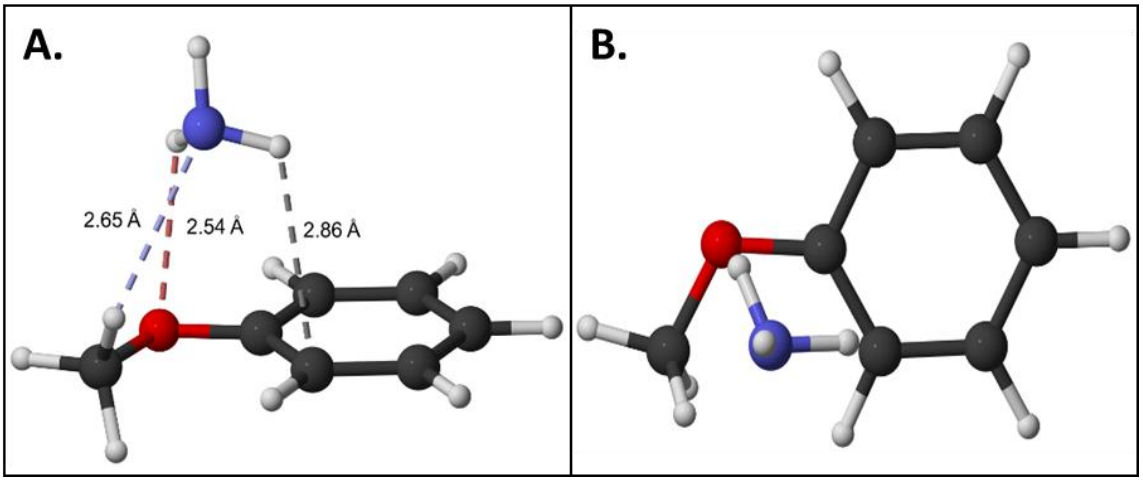

Figure A-3: The calculated ground-state structure for the anisole-NH_3 complex using M06-2X-D3/def2-QZVPPD method. The image on the left gives a side-on view while the image on the right gives a top-down view.

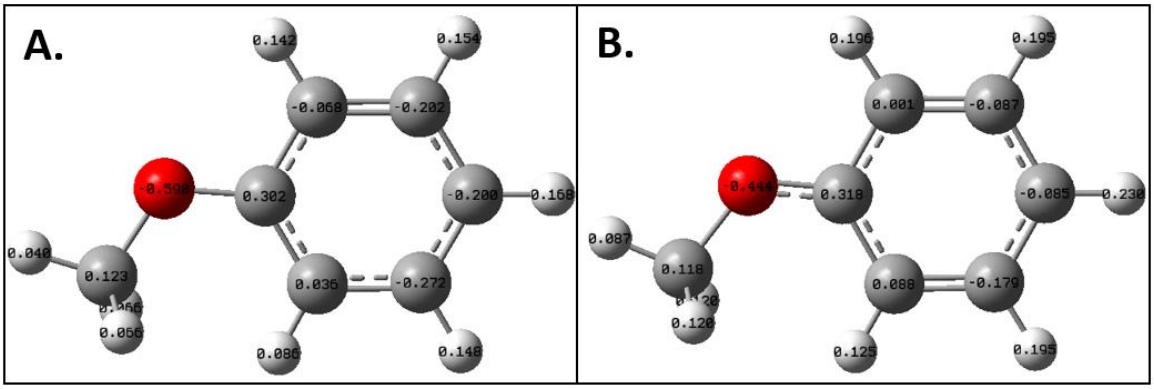

Figure A-4: The calculated Mulliken Charge maps for anisole using B3LYP-D3/def2-QZVPPD. A. gives the charge map for neutral anisole while B. gives the charge map for anisole in the cation radical state.

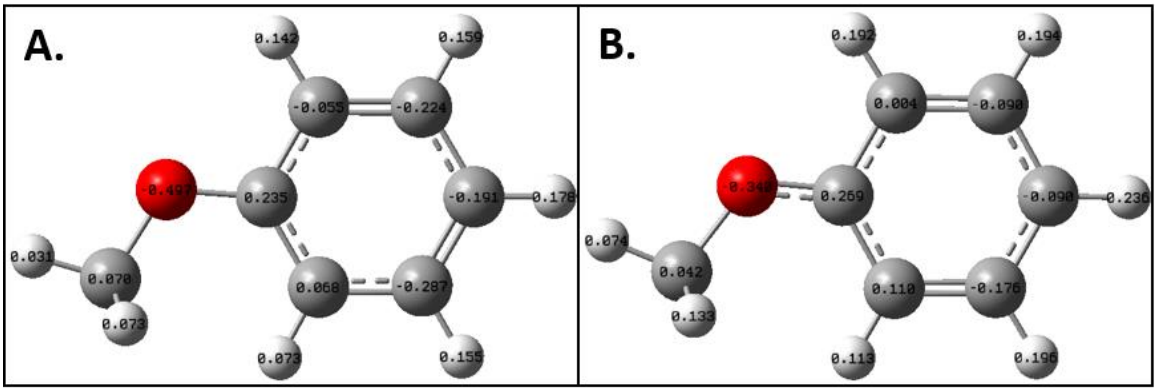

Figure A-5: The calculated Mulliken Charge maps for anisole using PBE0-D3/def2-QZVPPD. A. gives the charge map for neutral anisole while B. gives the charge map for anisole in the cation radical state.

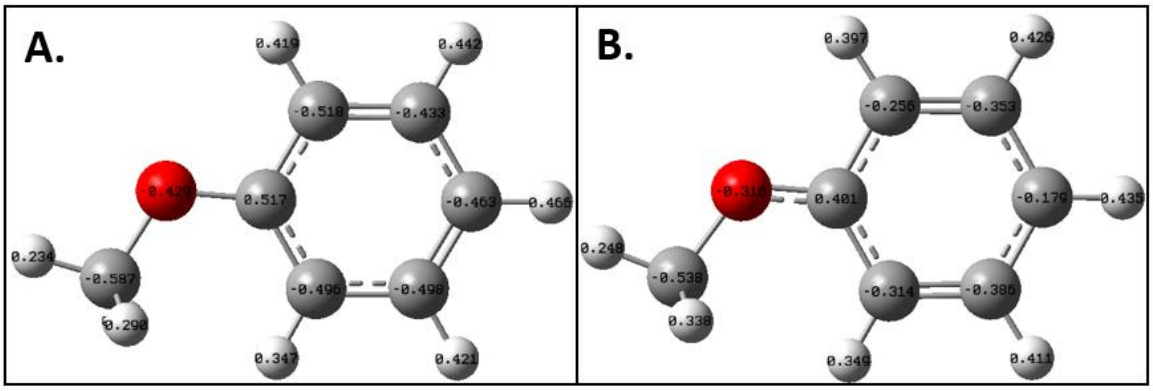

Figure A-6: The calculated Mulliken Charge maps for anisole using M06-2X-D3/def2-QZVPPD. A. gives the charge map for neutral anisole while B. gives the charge map for anisole in the cation radical state.

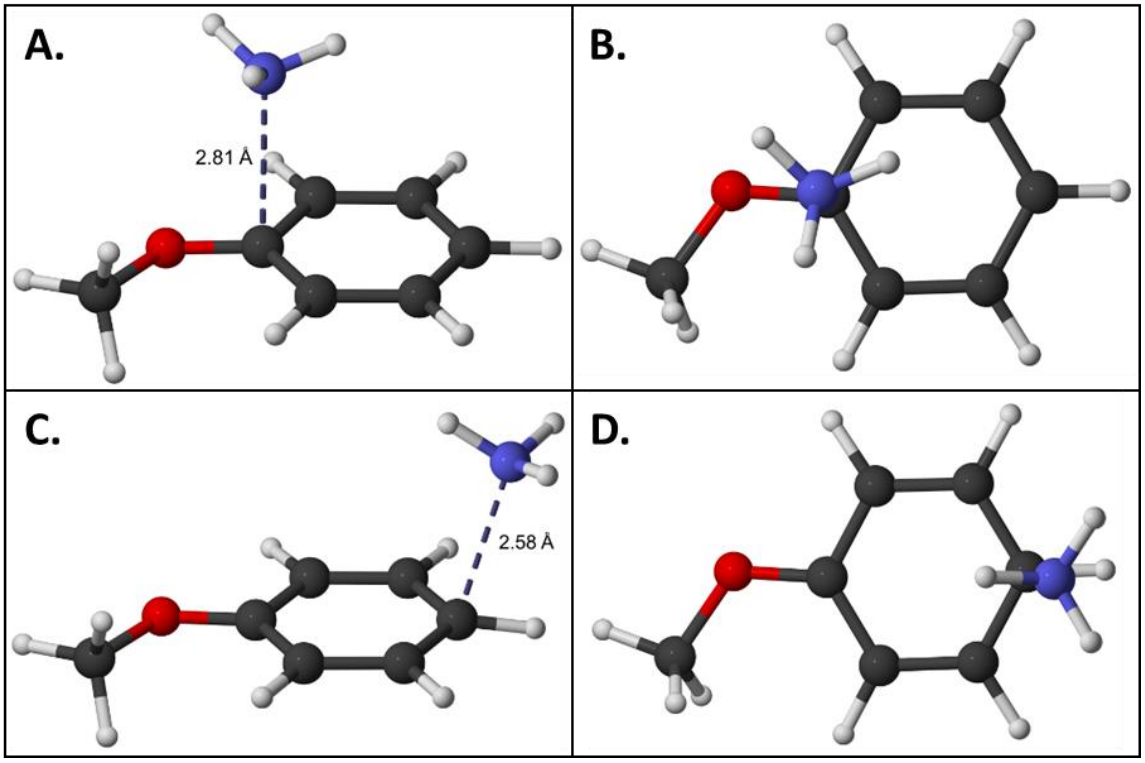

Figure A-7: The calculated cation-radical state conformers for the anisole-NH_3 complex using B3LYP-D3/def2-QZVPPD method. A. gives a side-on view of conformer #1 while B. gives a top-down view of conformer #1. C. gives a side-on view of conformer #2 while D. gives a top-down view of conformer #2.

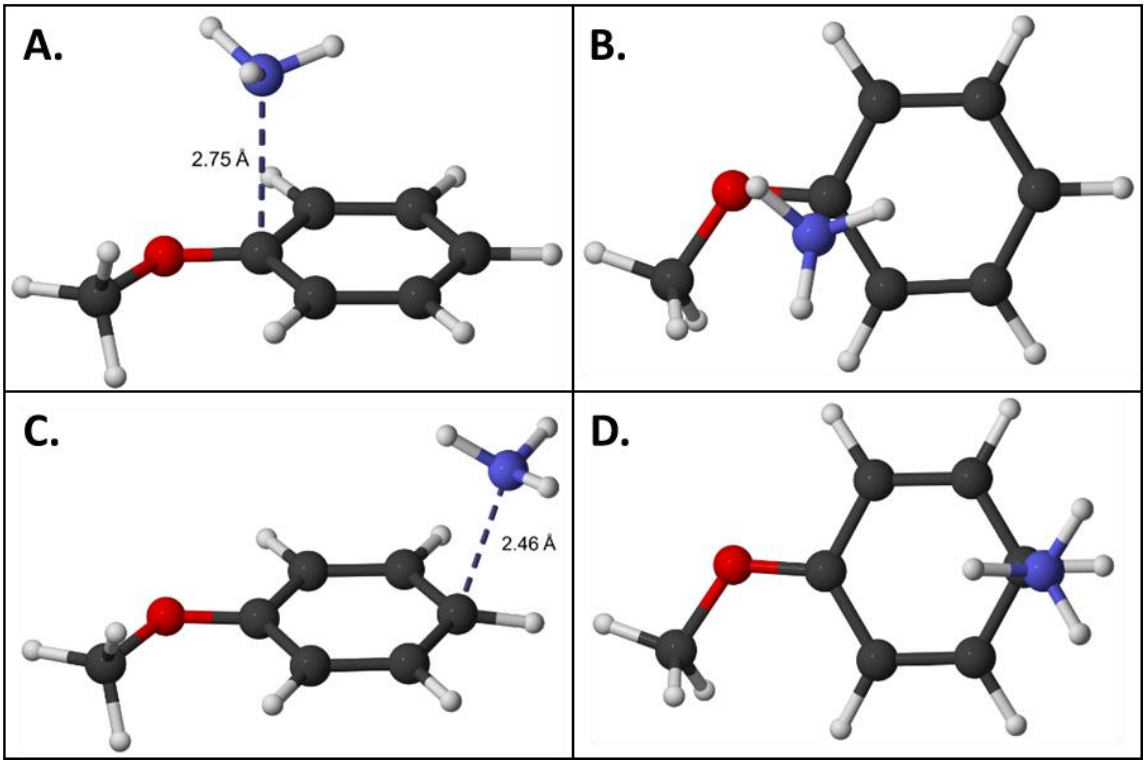

Figure A-8: The calculated cation-radical state conformers for the anisole-NH_3 complex using PBE0-D3/def2-QZVPPD method. A. gives a side-on view of conformer #1 while B. gives a top-down view of conformer #1. C. gives a side-on view of conformer #2 while D. gives a top-down view of conformer #2.

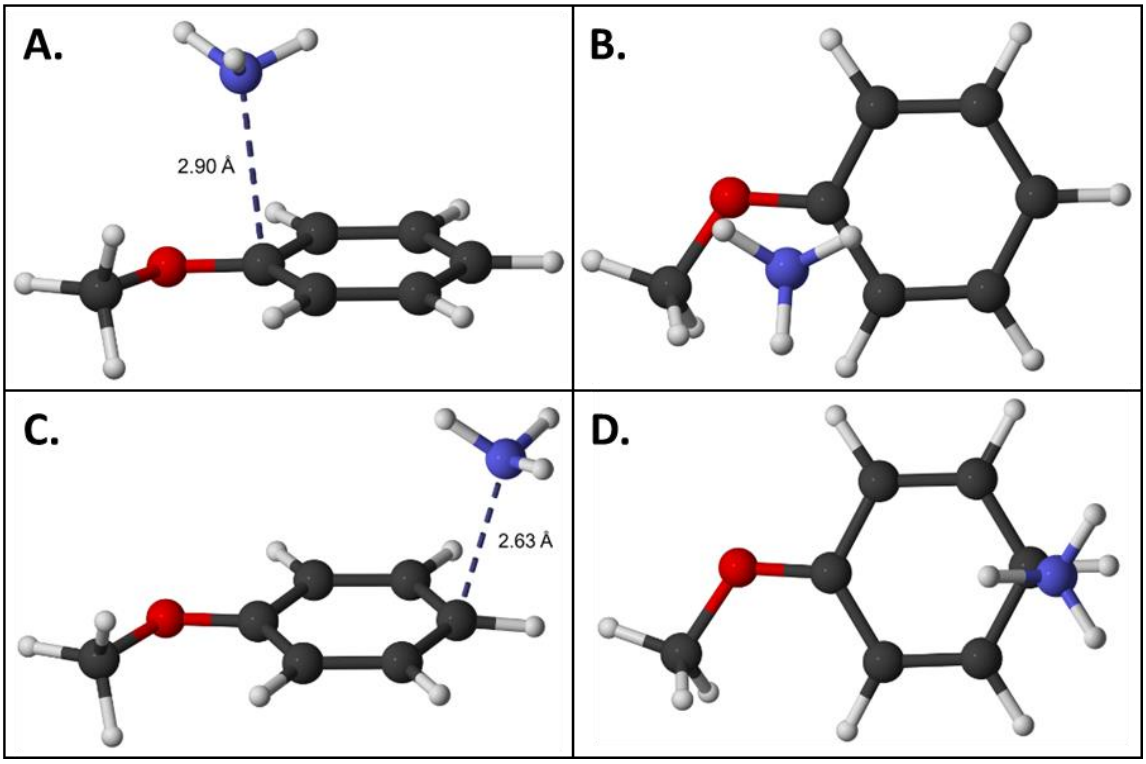

Figure A-9: The calculated cation-radical state conformers for the anisole-NH_3 complex using M06-2X-D3/def2-QZVPPD method. A. gives a side-on view of conformer #1 while B. gives a top-down view of conformer #1. C. gives a side-on view of conformer #2 while D. gives a top-down view of conformer #2.

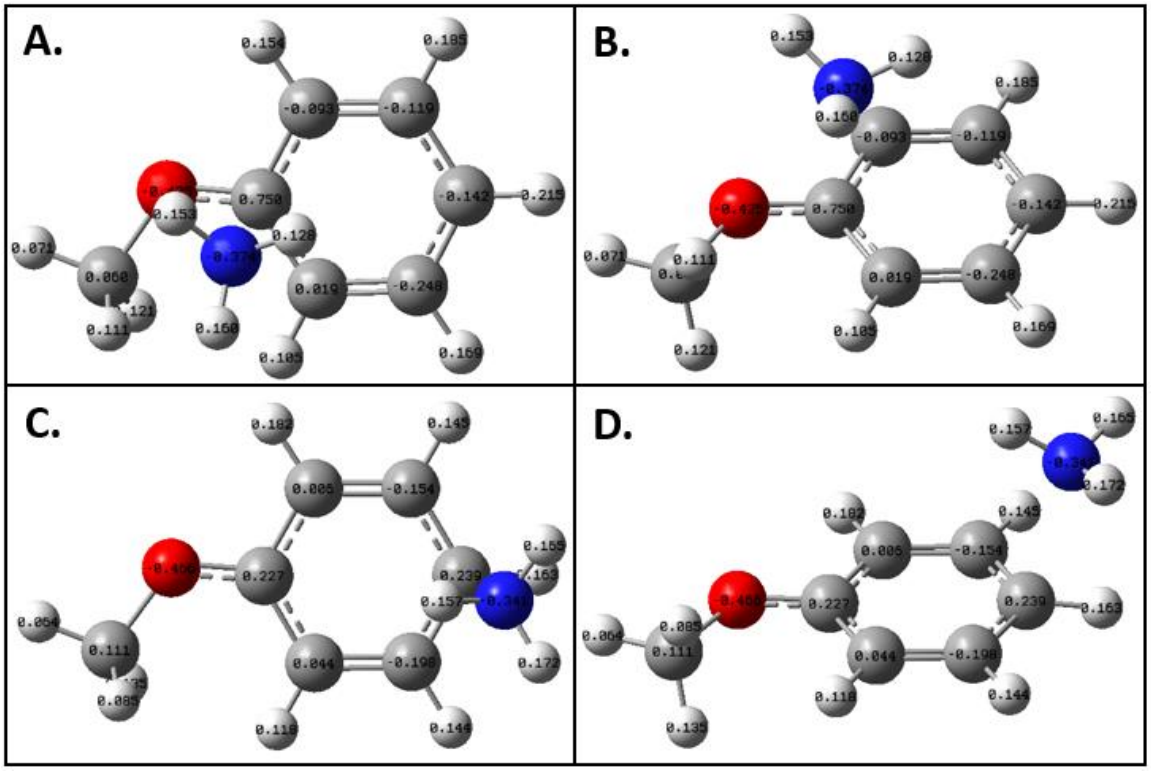

Figure A-10: The calculated Mulliken Charge maps for anisole-NH_3 cation radical conformers using B3LYP-D3/def2-QZVPPD. A. gives a side-on view of conformer #1 while B. gives a top-down view of conformer #1. C. gives a side-on view of conformer #2 while D. gives a top-down view of conformer #2.

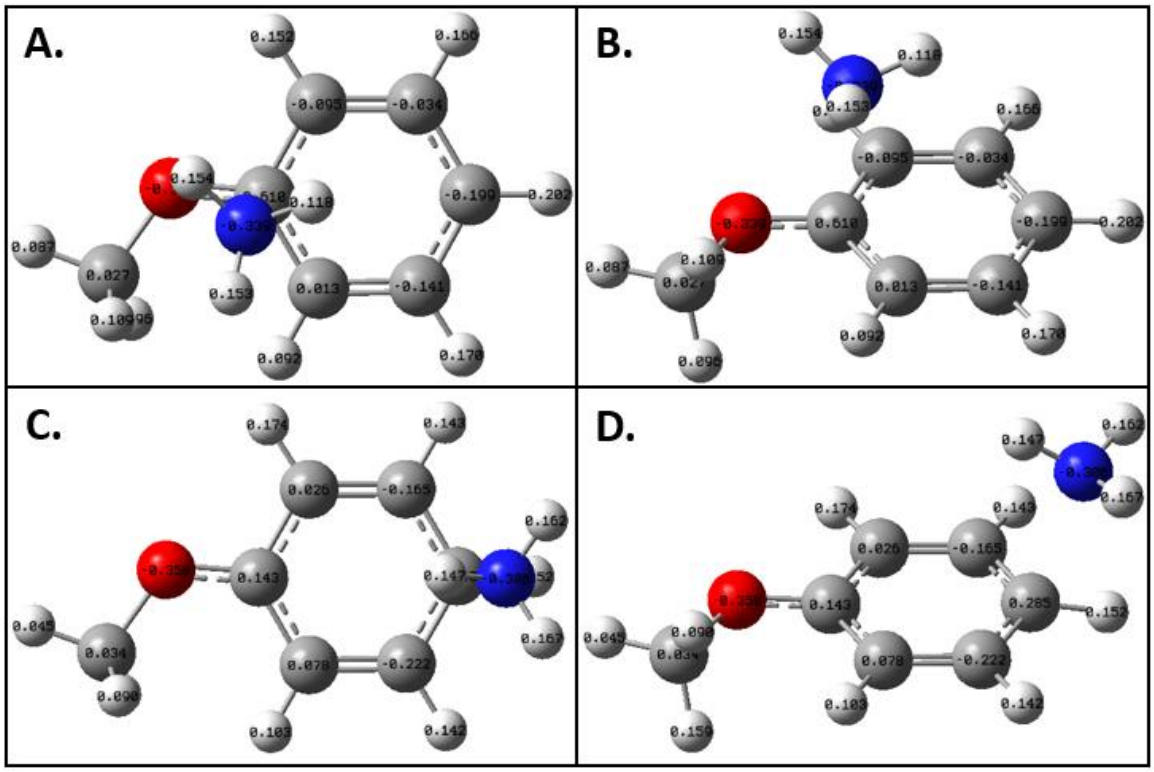

Figure A-11: The calculated Mulliken Charge maps for anisole-NH_3 cation radical conformers using PBE0-D3/def2-QZVPPD. A. gives a side-on view of conformer #1 while B. gives a top-down view of conformer #1. C. gives a side-on view of conformer #2 while D. gives a top-down view of conformer #2.

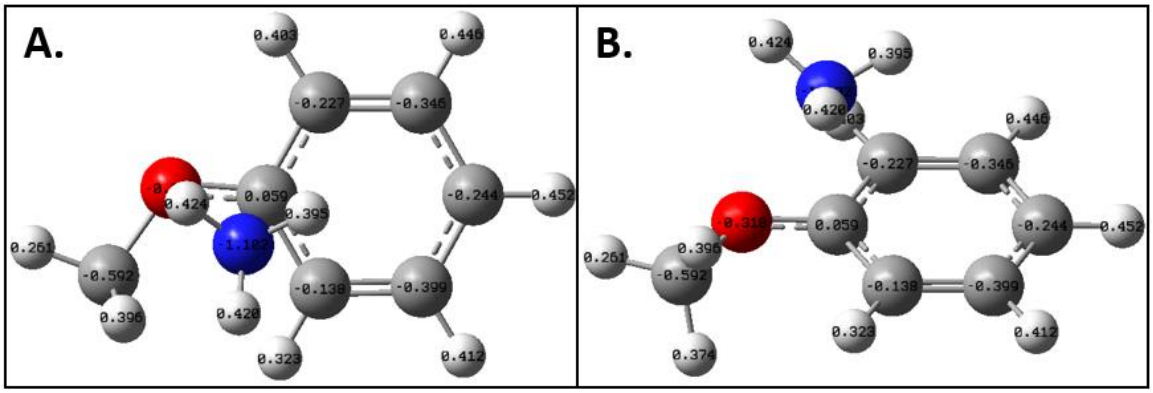

Figure A-12: The calculated Mulliken Charge maps for anisole-NH_3 cation radical conformer #1 using M06-2X-D3/def2-QZVPPD. A. gives a side-on view of the conformer while B. gives a top-down view of the conformer.

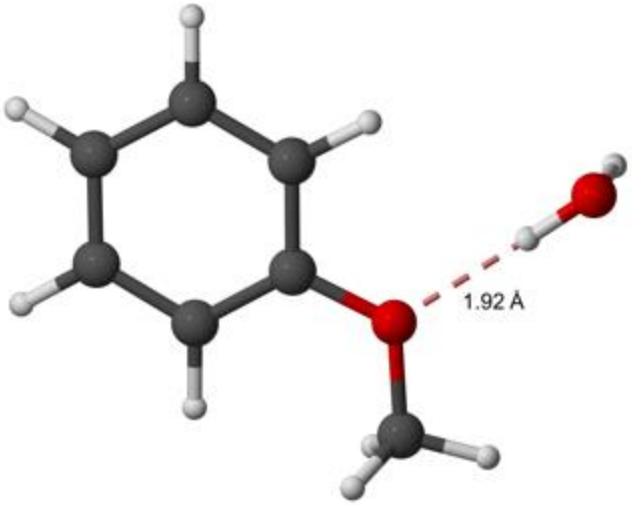

Figure A-13: The calculated ground-state structure for the anisole-H_2O complex using B3LYP-D3/def2-QZVPPD method.

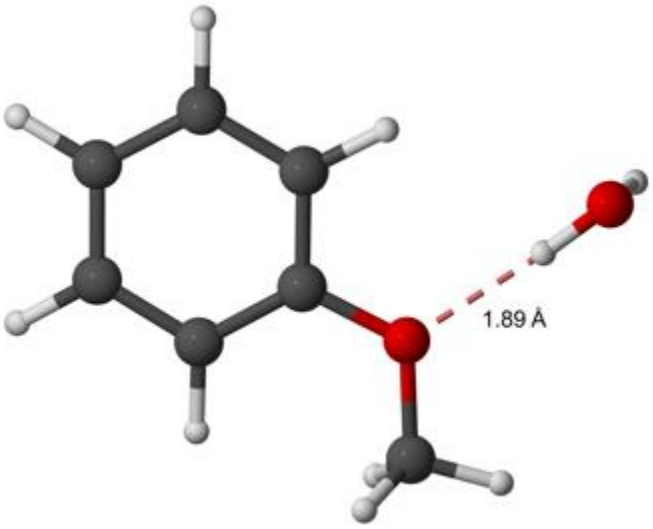

Figure A-14: The calculated ground-state structure for the anisole-H_2O complex using CAM-B3LYP-D3/def2-QZVPPD method.

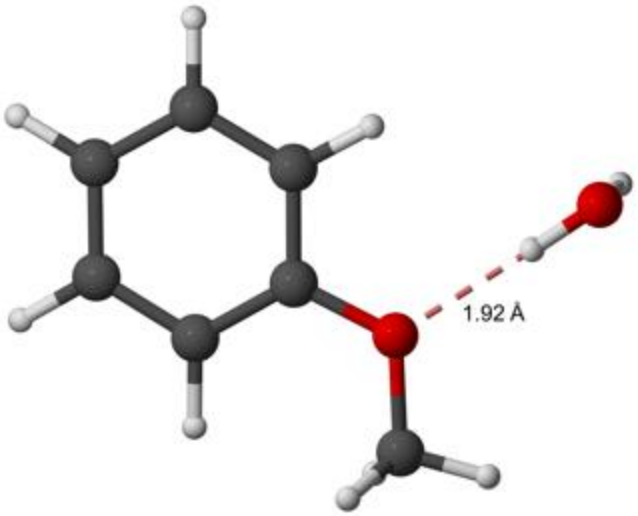

Figure A-15: The calculated ground-state structure for the anisole-H_2O complex using PBE0-D3/def2-QZVPPD method.

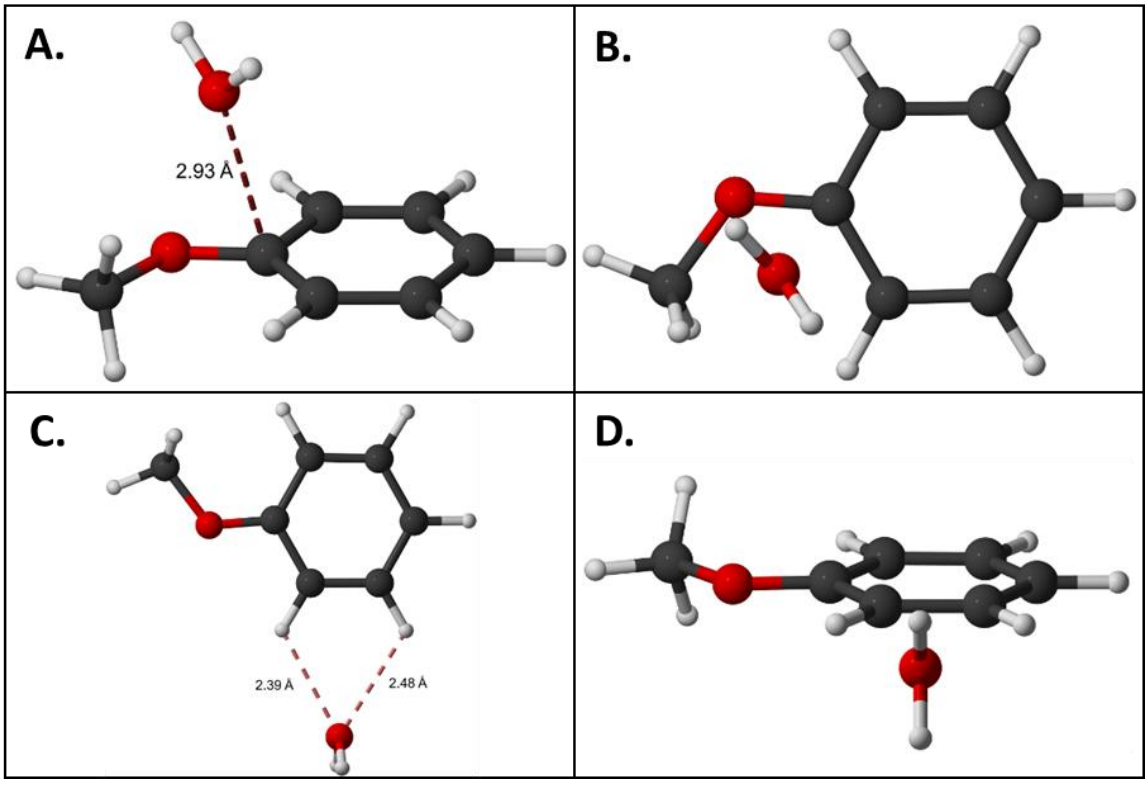

Figure A-16: The calculated cation-radical state conformers for the anisole-H_2O complex using CAM-B3LYP-D3/def2-QZVPPD method. A. gives a side-on view of conformer #1 while B. gives a top-down view of conformer #1. C. gives a side-on view of conformer #2 while D. gives a top-down view of conformer #2.

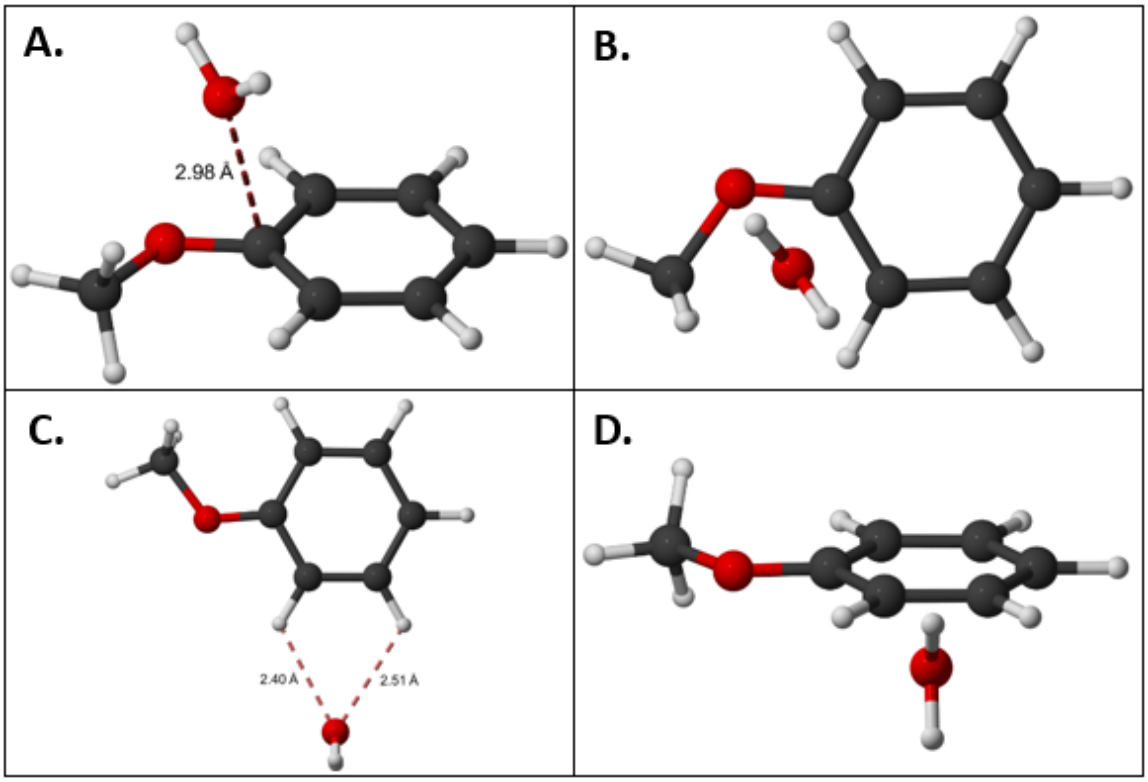

Figure A-17: The calculated cation-radical state conformers for the anisole-H_2O complex using PBE0-D3/def2-QZVPPD method. A. gives a side-on view of conformer #1 while B. gives a top-down view of conformer #1. C. gives a side-on view of conformer #2 while D. gives a top-down view of conformer #2.

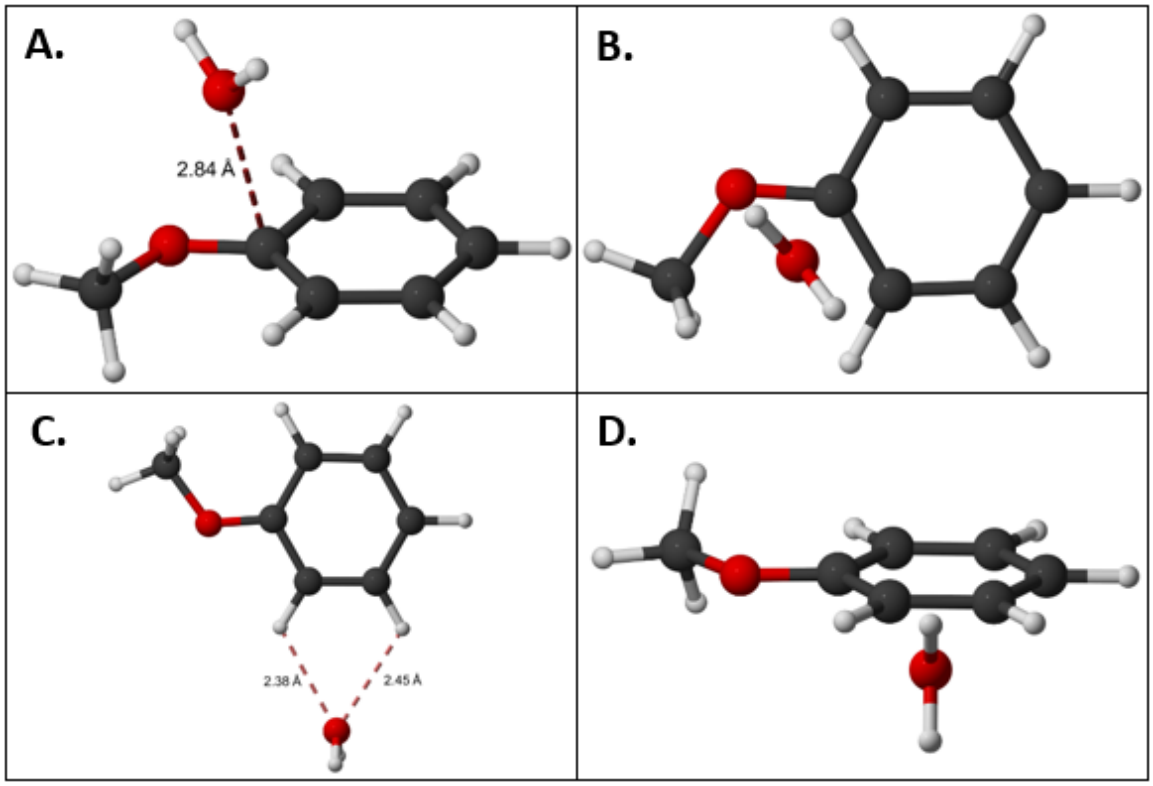

Figure A-18: The calculated cation-radical state conformers for the anisole-H_2O complex using M06-2X-D3/def2-QZVPPD method. A. gives a side-on view of conformer #1 while B. gives a top-down view of conformer #1. C. gives a side-on view of conformer #2 while D. gives a top-down view of conformer #2.

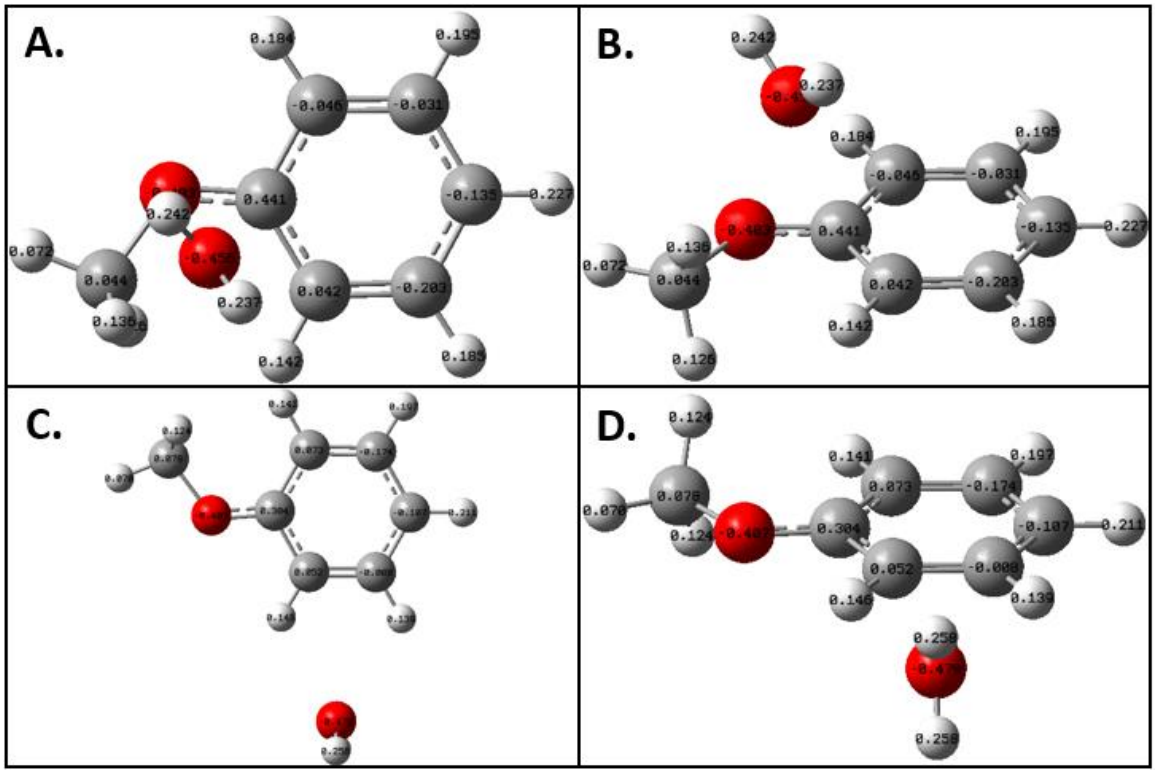

Figure A-19: The calculated Mulliken Charge maps for anisole-H_2O cation radical conformers using CAM-B3LYP-D3/def2-QZVPPD. A. gives a side-on view of conformer #1 while B. gives a top-down view of conformer #1. C. gives a side-on view of conformer #2 while D. gives a top-down view of conformer #2.

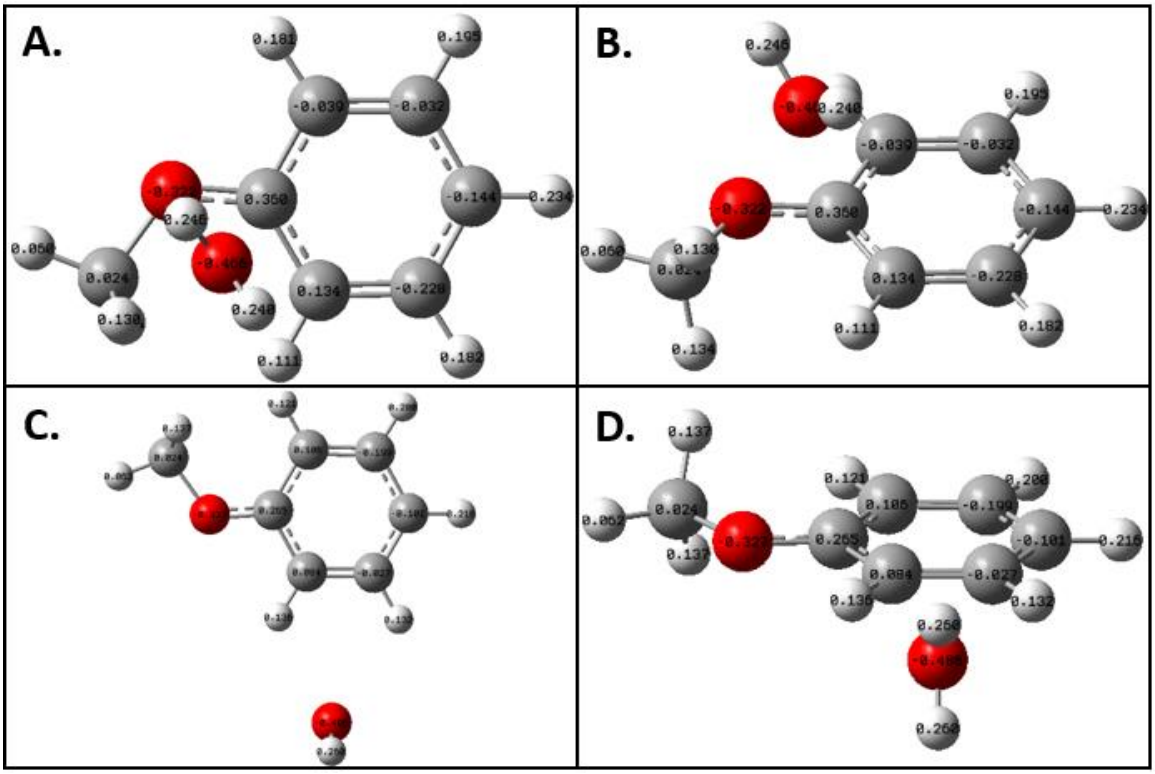

Figure A-20: The calculated Mulliken Charge maps for anisole-H_2O cation radical conformers using PBE0-D3/def2-QZVPPD. A. gives a side-on view of conformer #1 while B. gives a top-down view of conformer #1. C. gives a side-on view of conformer #2 while D. gives a top-down view of conformer #2.

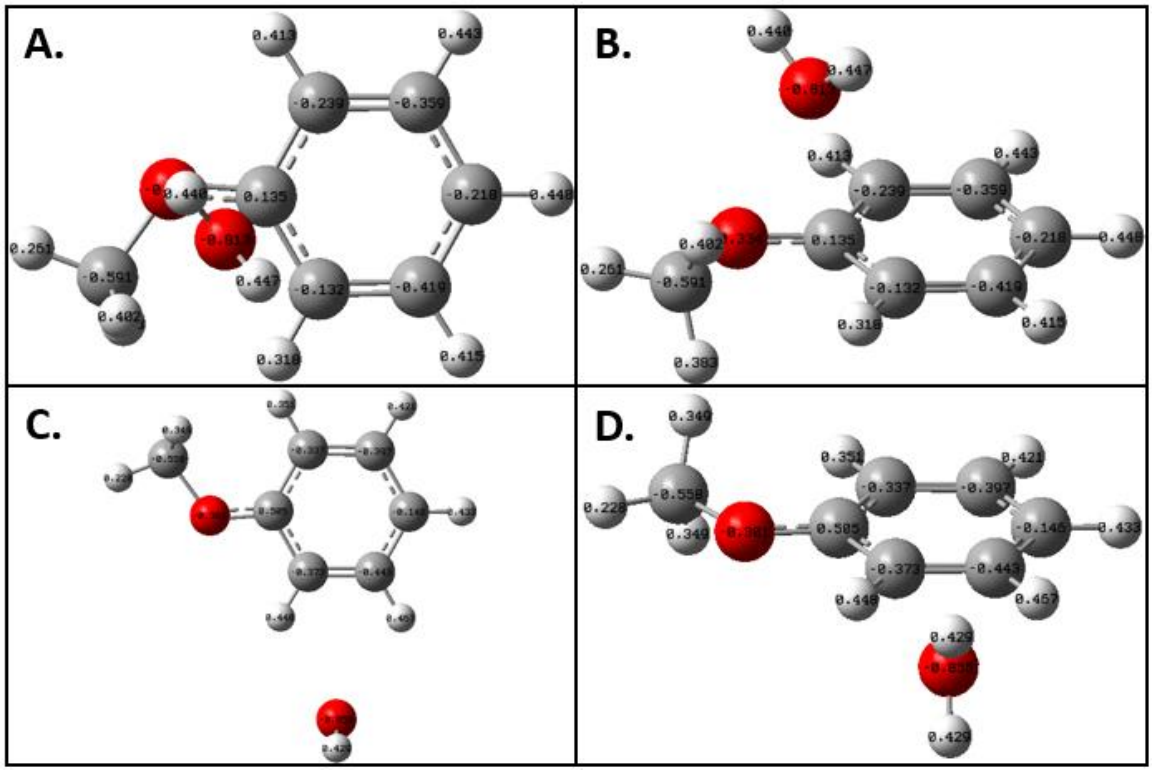

Figure A-21: The calculated Mulliken Charge maps for anisole-H_2O cation radical conformers using M06-2X-D3/def2-QZVPPD. A. gives a side-on view of conformer #1 while B. gives a top-down view of conformer #1. C. gives a side-on view of conformer #2 while D. gives a top-down view of conformer #2.

BIBLIOGRAPHY

1. Shang, Q. Y.; Bernstein, E. R. *Chem. Rev.* **1994**, *94*, 2015-2025.
2. Bernstein, E. R. *Annu. Rev. Phys. Chem.* **1995**, *46*, 197-222.
3. Sun, S.; Bernstein, E. R. *J. Phys. Chem.* **1996**, *100*, 13348–13366.
4. Rohrbacher, A.; Halberstadt, N.; Janda, K. C. *Annu. Rev. Phys. Chem.* **2000**, *51*, 405–433.
5. Müeller-Dethlefs, K.; Hobza, P. *Chem. Rev.* **2000**, *100*, 143–168.
6. Kim, K. S.; Tarakeshwar, P.; Lee, J. Y. *Chem. Rev.* **2000**, *100*, 4145–4186.
7. Dykstra, C. E.; Lisy, J. M. *Journal of Molecular Structure: Theochem* **2000**, *500*, 375-390.
8. Braun, J. E.; Mehnert, Th.; Neusser, H. J. *International Journal of Mass Spectrometry* **2000**, *203*, 1-18.
9. Hobza, P.; Zahradník, R.; Müeller-Dethlefs, K. *Collect. Czech. Chem. Commun.* **2006**, *71*, 443-531.
10. Samantha, A. K.; Wang, Y.; Mancini, J. S. et al. *Chem. Rev.* **2016**, *116*, 4913–4936.
11. Becucci, M.; Melandri, S. *Chem. Rev.* **2016**, *116*, 5014–5037.
12. Frey, J. A.; Holzer, C., Klopper, W. et al. *Chem. Rev.* **2016**, *116*, 5614–5641.
13. Stace, T. *Nature* **1987**, *327*, 186−187.
14. Buck, U. *Ber. Bunsen Phys. Chem.* **1992**, *96*, 1275−1284.
15. Jortner, J.; Even, U.; Goldberg, A. et al. *Surf. Rev. Lett.* **1996**, *3*, 263−280.
16. Herschbach, D. *Rev. Mod. Phys.* **1999**, *71*, S411−S418.
17. Riley, K. E.; Pitoňák, M.; Jurečka, P. et al. *Chem. Rev.* **2010**, *110*, 5023–5063.
18. Řezáč, J.; Hobza, P. *Chem. Rev.* **2016**, *116*, 5038–5071.
19. Vosko, S. H.; Wilk, L.; Nusair, M. *Can. J. Phys.* **1980**, *58*, 1200-1211.

20. Lee, C. T.; Yang, W. T.; Parr, R. G. *Phys. Rev. B* **1988**, *37,* 785-789.

21. Becke, A. D. *J. Chem. Phys.* **1993**, *98,* 5648-5652.

22. Stephens, P. J.; Devlin, F. J.; Chabalowski, C. F. et al. *J. Phys. Chem.* **1994**, *98,* 11623-11627.

23. Yanai, T.; Tew, D.; Handy, N. *Chem. Phys. Lett.* **2004**, *393,* 51-57.

24. Peach, M. J. G.; Helgaker, T.; Salek, P. et al. *Phys. Chem. Chem. Phys.* **2006**, *8,* 558-562.

25. Chai, J. -D.; Head-Gordon, M. *Phys. Chem. Chem. Phys.* **2008**, *10,* 6615-6620.

26. Zhao, Y.; Truhlar, D. G. *Theor. Chem. Acc.* **2008**, *120,* 215-241.

27. Zhao, Y.; Truhlar, D. G. *J. Phys. Chem. A* **2005**, *109,* 5656.

28. Perdew, J. P.; Burke, K.; Ernzerhof, M. *Phys. Rev. Lett.* **1996**, *77,* 3865-3868.

29. Perdew, J. P.; Burke, K.; Ernzerhof, M. *Phys. Rev. Lett.* **1997**, *78,* 1396-1396.

30. Grimme, S.; Antony, J.; Ehrlich, S. et al. *J. Chem. Phys.* **2010**, *132,* 154104.

31. Grimme, S.; Ehrlich, S.; Goerigk, L. *J. Comput. Chem.* **2011**, *32,* 1456-1465.

32. Nauta, K.; Miller, R. E. *Science* **2000**, *287,* 293.

33. Rocher-Casterline, B. E.; Ch'ng, L. C.; Mollner, A. K. et al. *J. Chem. Phys.* **2011**, *134,* 211101.

34. Shank, A.; Wang, Y.; Kaledin, A. et al. *J. Chem. Phys.* **2009**, *130,* 144314.

35. Nelson, D. D.; Fraser, G. T.; Klemperer, W. *J. Chem. Phys.* **1985**, *83,* 6201−6208.

36. Nelson, D. D.; Klemperer, W.; Fraser, G. T. et al *J. Chem. Phys.* **1987**, *87,* 6364−6372.

37. Havenith, M.; Cohen, R. C.; Busarow, K. L. et al. *J. Chem. Phys.* **1991**, *94,* 4776−4789.

38. Loeser, J. G.; Schmuttenmaer, C. A.; Cohen, R. C. et al. *J. Chem. Phys.* **1992**, *97,* 4727−4749.

39. van Bladel, J. W. I.; van der Avoird, A.; Wormer, P. E. S. et al. *J. Chem. Phys.* **1992**, *97,* 4750−4763.

40. Case, A. S.; Heid, C. G.; Kable, S. H. et al. *J. Chem. Phys.* **2011**, *135*, 084312.

41. Slipchenko, M. N.; Sartakov, B. G.; Vilesov, A. F. et al. *J. Phys. Chem. A* **2007**, *111*, 7460– 747.

42. Janeiro-Barral, P. E.; Mella, M. *J. Phys. Chem. A* **2006**, *110,* 11244– 11251.

43. Rodham, D. A.; Suzuki, S.; Suenram, R. D. et al. *Nature* **1993**, *362,* 735.

44. Mons, M.; Dimicoli, I.; Tardive, B. et al. *Phys. Chem. Chem. Phys.* **2002**, *4,* 571-576.

45. Wanna, J.; Menapace, J. A.; Bernstein, E. R. *J. Chem. Phys.* **1986**, *85,* 1795-1805.

46. Vaupel, S.; Brutschy, B.; Tarakeshwar, P. et al. *J. Am. Chem. Soc.* **2006**, *128,* 5416-5426.

47. Cheng, B.-M.; Grover, J. R.; Walters, E. A. *Chem. Phys. Lett.* **1995**, *232,* 364-369.

48. Fredericks, S. Y.; Jordan, K. D; Zwier, T. S. *J. Phys. Chem.* **1996**, *100,* 7810-7821.

49. Reid, S. A.; Nyambo, S.; Kalume, A. et al. *J. Phys. Chem. A* **2013**, *117,* 12429-12437.

50. Tongue, N. M.; MacMahon, E. C.; Pugliesi, I. et al. *J. Chem. Phys.* **2007**, *126,* 154319.

51. Brendel, K.; Mäder, H.; Xu, Y. et al. *J. Mol. Spec.* **2011**, *268,* 47-52.

52. Giuliano, B. M.; Evangelisti, L.; Maris, A. et al. *Chem. Phys. Lett.* **2010**, *485*, 36-39.

53. Spada, L.; Tasinato, N.; Vazart, F. et al. *Chem. Eur. J.* **2017**, *23,* 4876-4883.

54. Mackenzie, R. B.; Dewberry, C. T.; Cornelius, R. D. et al. *J. Phys. Chem. A* **2017**, *121*, 855–860.

55. Berden, G.; Meerts, W. L.; Schmitt, M. et al. *J. Chem. Phys.* **1996**, *104,* 972-982.

56. Gerhards, M.; Schmitt, M.; Kleinermanns, K. et al. *J. Chem. Phys.* **1996**, *104,* 967-971.

57. Henseler, D.; Tanner, C., Frey, H. et al. *J. Chem. Phys.* **2001**, *115,* 4055-4069.

58. Yoshino, R.; Hashimoto, K.; Omi, T et al. *J. Phys. Chem. A* **1998**, *102,* 6227–6233.

59. Knochenmuss, R.; Karbach, V.; Wickleder, C et al. *J. Phys. Chem. A* **1998**, *102,* 1935−1944.

60. Fernandez, J. A.; Bernstein, E. R. *J. Chem. Phys.* **1997**, *108,* 3029-3037.

61. Spoerel, U.; Stahl, W. *J. Mol. Spec.* **1998**, *190,* 278-289.

62. Piani, G.; Pasquini, M.; López-Tocón, I. et al. *Chem. Phys.* **2006**, *330,* 138-145.

63. Piani, G.; Pasquini, M.; Pietraperzia, G. et al. *Chem. Phys. Lett.* **2007**, *434,* 25-30.

64. Biczysko, M.; Piani, G.; Pasquini, M. et al. *J. Chem. Phys.* **2007**, *127,* 144303.

65. Barone, V.; Biczysko, M.; Pavone, M. *Chemical Physics* **2008**, *346,* 247-256.

66. Guiliano, B. M.; Maris, A.; Melandri, S. et al. *J. Phys. Chem. A* **2009**, *113,* 14277-14280.

67. Barth, H.-D.; Buchhold, K.; Djafari, S. et al. *Chemical Physics* **1998**, *239,* 49-64.

68. Reimann, B.; Buchhold, K.; Barth, H.-D. et al. *J. Phys. Chem.* **2002**, *117,* 8805-8822.

69. Becucci, M.; Pietraperzia, G.; Pasquini, M. et al. *J. Chem. Phys.* **2004**, *120*, 5601-5607.

70. Pietraperzia, G.; Chelli, R.; Becucci, M. et al. *Molecular Mechanics and Dynamics Calculations to Bridge Molecular Structure Information and Spectroscopic Measurements on Complexes of Aromatic Compounds,* Proceedings of ICCSA, Assisi, Italy May 14-17, **2004**.

71. Guiliano, B. M.; Caminati, W. *Angew. Chem. Int. Ed.* **2005**, *44*, 603-606.

72. Guiliano, B. M.; Melandri, S.; Caminati, W. *Journal of Molecular Spectroscopy* **2017**, *337,* 86-89.

73. Ribblett, J. W.; Sinclair, W. E.; Borst; D. R. et al. *J. Phys. Chem. A* **2006,** *110,* 1478-1483.

74. Pasquini, M.; Schiccheri, N.; Piani G. et al. *J. Phys. Chem. A* **2007**, *111*, 12363-12371.

75. Muzangwa, L.; Nyambo, S.; Uhler, B. et al. *J. Chem. Phys.* **2012**, *137*, 184307.

76. Frisch, M. J.; Trucks, G. W.; Schlegel, H. B. et al. Gaussian 16, Revision B.01; Gaussian, Inc. Wallingford, CT, 2016.

77. Towns, J.; Cockerill, T.; Dahan, M. et al. *Computing in Science & Engineering* **2014**, *16*, 62-74.

78. Weigend, F.; Furche, F.; Ahlrichs, R. *J. Chem. Phys.* **2003**, *119*, 12753-12762.

79. Rappoport, D.; Furche, F. *J. Chem. Phys.* **2010**, *133*, 134105.

80. Makuvaza, J. T.; Kokkin, D. L.; Loman, J. L. et al. *J. Phys. Chem. A* **2019**, *123*, 2874-2880.

81. Duncan, J. L.; Mills, I. M. *Spectrochimica Acta* **1964**, *20*, 523-546.

82. Schäfer, M.; Borst, D. R.; Pratt, D. W. et al. *Mol. Phys.* **2002**, *100*, 3553.

83. Kang, C.-H.; Pratt, D. W.; Schäfer, M. *J. Phys. Chem. A* **2005**, *109*, 767.

84. Korter, T. M.; Pratt, D. W.; Küpper, J. *J. Phys. Chem. A* **1998**, *102*, 7211.

85. Makuvaza, J. T.; Loman, J. L.; Kokkin, D. L. et al. *J. Chem. Phys.* **2020**, *153*, 044303.